



# Galaninergic and hypercapnia-activated neuronal projections to the ventral respiratory column

Ayse S. Dereli<sup>1</sup> · Alice Y. S. Oh<sup>1</sup> · Simon McMullan<sup>2</sup> · Natasha N. Kumar<sup>1</sup>

Received: 27 December 2023 / Accepted: 26 February 2024  
© The Author(s) 2024

## Abstract

In mammals, the ventral respiratory column (VRC) plays a pivotal role in integrating neurochemically diverse inputs from brainstem and forebrain regions to generate respiratory motor patterns. VRC microinjection of the neuropeptide galanin has been reported to dampen carbon dioxide (CO<sub>2</sub>)-mediated chemoreflex responses. Additionally, we previously demonstrated that galaninergic neurons in the retrotrapezoid nucleus (RTN) are implicated in the adaptive response to hypercapnic stimuli, suggesting a link between RTN neuroplasticity and increased neuronal drive to the VRC. VRC neurons express galanin receptor 1, suggesting potential regulatory action by galanin, however, the precise galaninergic chemoreceptor-VRC circuitry remains to be determined. This study aimed to identify sources of galaninergic input to the VRC that contribute to central respiratory chemoreception. We employed a combination of retrograde neuronal tracing, *in situ* hybridisation and immunohistochemistry to investigate VRC-projecting neurons that synthesise galanin mRNA. In an additional series of experiments, we used acute hypercapnia exposure (10% CO<sub>2</sub>, 1 h) and *c-Fos* immunohistochemistry to ascertain which galaninergic nuclei projecting to the VRC are activated. Our findings reveal that a total of 30 brain nuclei and 51 subnuclei project to the VRC, with 12 of these containing galaninergic neurons, including the RTN. Among these galaninergic populations, only a subset of the RTN neurons (approximately 55%) exhibited activation in response to acute hypercapnia. Our findings highlight that the RTN is the likely source of galaninergic transmission to the VRC in response to hypercapnic stimuli.

**Keywords** Galanin · Ventral respiratory column · Neuronal tracing · Breathing regulation · Central chemoreception · *c-Fos*

## Introduction

Located within the ventrolateral medulla, the ventral respiratory column (VRC) plays a crucial role in generating and regulating respiratory motor patterns. The VRC consists of four distinct compartments: Bötzing Complex (BötC), preBötzing Complex (preBötC), rostral ventral respiratory

group (rVRG), and caudal ventral respiratory group (cVRG) (Guyenet et al. 2019). The BötC and preBötC together form the central respiratory pattern generator. Specifically, the preBötC is responsible for the intrinsic rhythmicity of inspiration (Feldman and Del Negro 2006; Koshiya and Smith 1999; Rekling and Feldman 1998; Smith et al. 2000, 1991), while the BötC is responsible for sculpting the expiratory phase of the respiratory cycle (Ezure 1990; Ezure et al. 2003; Jiang and Lipski 1990; Tian et al. 1999). This rhythmic activity is relayed to premotor neurons in the rVRG, which contains bulbospinal inspiratory excitatory neurons that are driven by the preBötC during inspiration and inhibited by BötC neurons during expiration (Smith et al. 2009), and the cVRG, which contains bulbospinal expiratory excitatory neurons, presumed to serve as the expiratory counterpart to the inspiratory rVRG (Smith et al. 2009).

Central respiratory pattern generation requires intricate neuronal interactions; both *in vivo* and *in vitro* voltage clamp techniques demonstrate that this mechanism relies on synaptic interaction, characterised by excitatory glutamatergic

✉ Natasha N. Kumar  
natasha.kumar@unsw.edu.au

Ayse S. Dereli  
ayse.dereli@uclouvain.be

Alice Y. S. Oh  
yunsu.oh@student.unsw.edu.au

Simon McMullan  
simon.mcmullan@mq.edu.au

<sup>1</sup> Department of Pharmacology, School of Biomedical Sciences, University of New South Wales, Sydney, Australia

<sup>2</sup> Macquarie Medical School, Macquarie University, Sydney, Australia

synaptic activation through AMPA and NMDA receptors. Whereas inhibitory GABA<sub>A</sub>, GABA<sub>B</sub> and glycine receptor-mediated synaptic inputs sculpt the burst pattern (Busselberg et al. 2001; Richter et al. 1996).

Beyond the roles of fast transmitters in the respiratory central pattern generator, pharmacological and immunohistochemical studies have revealed that the VRC possesses receptors for a range of signalling molecules, including vasopressin (Kc et al. 2002), oxytocin (Mack et al. 2007), substance P (Gray et al. 1999; Langer et al. 2017b; Liu et al. 2004; Muere et al. 2015a, b),  $\mu$ -opioid, (Gray et al. 1999; Langer et al. 2017a), 5-HT (Langer et al. 2017b; Muere et al. 2015b; Ptak et al. 2009), somatostatin (Le et al. 2016; Burke et al. 2010), neuromedin B (Li et al. 2016) gastrin releasing peptide (Li et al. 2016) and galanin (Dereli et al. 2019). Thus, various neurotransmitter systems are implicated in the regulation of breathing.

A combination of *in vivo* and *in vitro* local acidification, c-Fos immunohistochemistry, genetic investigations and pharmacological studies, showed that central chemoreception mechanisms modulate the respiratory behaviour. Specifically, the retrotrapezoid nucleus (RTN), nucleus tractus solitarius (NTS), raphe, periaqueductal grey area (PAG) and lateral parabrachial nucleus (LPB) contain carbon dioxide (CO<sub>2</sub>)-responsive neurons (Damasceno et al. 2014; Kaur et al. 2013; Nattie and Li 2012; Yokota et al. 2015). Focal acidification studies show that the RTN, NTS, locus coeruleus (LC) and dorsomedial hypothalamic nucleus (DMH) have increased firing rate in response to decrease in pH with an increase in ventilation (Nattie and Li 2002, 2010, 2012). Another body of work showed that these populations have increased c-Fos immunoreactivity in response to high levels of PaCO<sub>2</sub> (Spirovski et al. 2012). Furthermore, studies in animal and human models showed that there is decreased ventilatory response to chronic hypercapnia implicating plasticity in the respiratory chemoreflex circuit (Burgraff et al. 2018; Schaefer 1963; Schaefer et al. 1963). Therefore, central respiratory chemoreception and associated brain regions have various roles in the control of breathing, however despite these findings, there remains gaps in our understanding about the neurochemistry and neural circuit underlying these functions.

We have previously demonstrated that galanin is a mediator for adaptive changes in the respiratory chemoreflex circuit during chronic CO<sub>2</sub> (Dereli et al. 2019). Galanin is an inducible peptidergic neuromodulator and galanin mRNA is expressed in many central respiratory chemoreceptor populations including the RTN, NTS, LC and lateral hypothalamic area (Nattie and Li 2002, 2010, 2012; Spirovski et al. 2012). Our results showed that following long term hypercapnia, galaninergic neurons in the RTN exhibited altered gene expression compared to room air control conditions and retained their central chemoreflex sensitivity as measured by

c-Fos expression (Dereli et al. 2019). Moreover, microinjection of galanin into the preBötC attenuates ventilation and induces apnoea (Abbott et al. 2009), and we have demonstrated that galanin receptor 1 is expressed in the preBötC, serving as a substrate for these effects (Dereli et al. 2019). Taken together, there is strong evidence for the role of galanin in CO<sub>2</sub> stimulated regulation of breathing.

The overall goal of this study is to identify and characterise neurons targeting the VRC. The preBötC, which forms the core of the respiratory rhythm generating circuitry within the VRC, is of particular interest. Due to its inherent rhythmic pacemaker-like properties, and role as a primary source of spontaneous inspiratory drive to premotor circuits, it emerges as a highly suitable target (Smith et al. 2009). Previous tracing studies demonstrated RTN projections to the preBötC in the mouse (Shi et al. 2021) and rat (Bochorishvili et al. 2012; Rosin et al. 2006). However, the neurochemistry and function of these projections still require further investigations. Although respiratory chemoresponsive areas containing galaninergic neuronal populations (namely the RTN, NTS, LC and lateral hypothalamic area) are recognised, along with the presence of galanin receptors expressed in the VRC, whether galanin projections to the VRC facilitate respiration remains unknown. Given the existing knowledge gaps, our hypothesis posits that multiple galaninergic brain regions project to the VRC, including areas involved in CO<sub>2</sub> stimulated breathing. Consequently, our study aims to achieve the following objectives: (1) Employ a mapping approach to identify all the brain projections to the VRC using a retrograde tracer centred into the preBötC. (2) Identify all galaninergic projections to the VRC. (3) Quantify the responsiveness of these VRC projections to acute hypercapnia through the assessment of c-Fos immunoreactivity.

Our findings collectively reveal that out of the 30 brain nuclei comprising 51 subnuclei that project to the VRC, only the RTN was recruited by the hypercapnia chemoreflex as indicated by c-Fos immunoreactivity. Furthermore, galaninergic inputs to the VRC originated from a limited number of nuclei out of which only the galaninergic RTN subset demonstrated significant neuronal activation in response to acute hypercapnia.

## Materials and methods

### Animals

All experimental procedures were approved by the Macquarie University Animal Ethics Committee (2018/024 and 2016/028) and carried out in accordance with the Australian Code of Practice for the Care and Use of Animals for Scientific Purposes and the National Health and Medical Research Council guidelines. Animals were group housed in

conventional caging with 12:12 h, light:dark cycle at 23 °C with ad libitum access to standard chow and water.

### Retrograde tracer microinjections into the VRC

Anaesthesia was induced with 5% isoflurane in oxygen and maintained with 1–3% isoflurane. Once in the surgical plane of anaesthesia, mice were treated with prophylactic analgesia (Carprofen, 5 mg/kg, s.c.) and antibiotics (Cephazolin, 100 mg/kg, i.m.) and placed on a heating pad (~37 °C). Subcutaneous local anaesthetic (bupivacaine, 0.5%, 0.1 ml) was injected around the skull surface and an incision was made to expose the skull sutures. The overlying connective tissue was cleared, the skull flattened, and a small hole drilled,

using a Neurostar stereotaxic robot, over the VRC (centered on the preBötC) ; 2.9 mm caudal to lambda and 1.3 mm lateral to midline.

A 20 nl unilateral injection of cholera toxin B (CTB) was pneumatically injected over 3–5 min into the VRC using a glass capillary micropipette of diameter 20–40 µm at 6.2 mm deep to lambda (1%; List Biological, Campbell, CA) (Fig. 1). The pipette was left in place for 5 min before withdrawal. At the conclusion of injections, the incision was closed with silk sutures, isoflurane was discontinued, and once ambulatory, animals were returned to their home cage for 3–5 days to allow for CTB transport. Carprofen (5 mg/kg, s.c.) was administered once daily for pain relief.

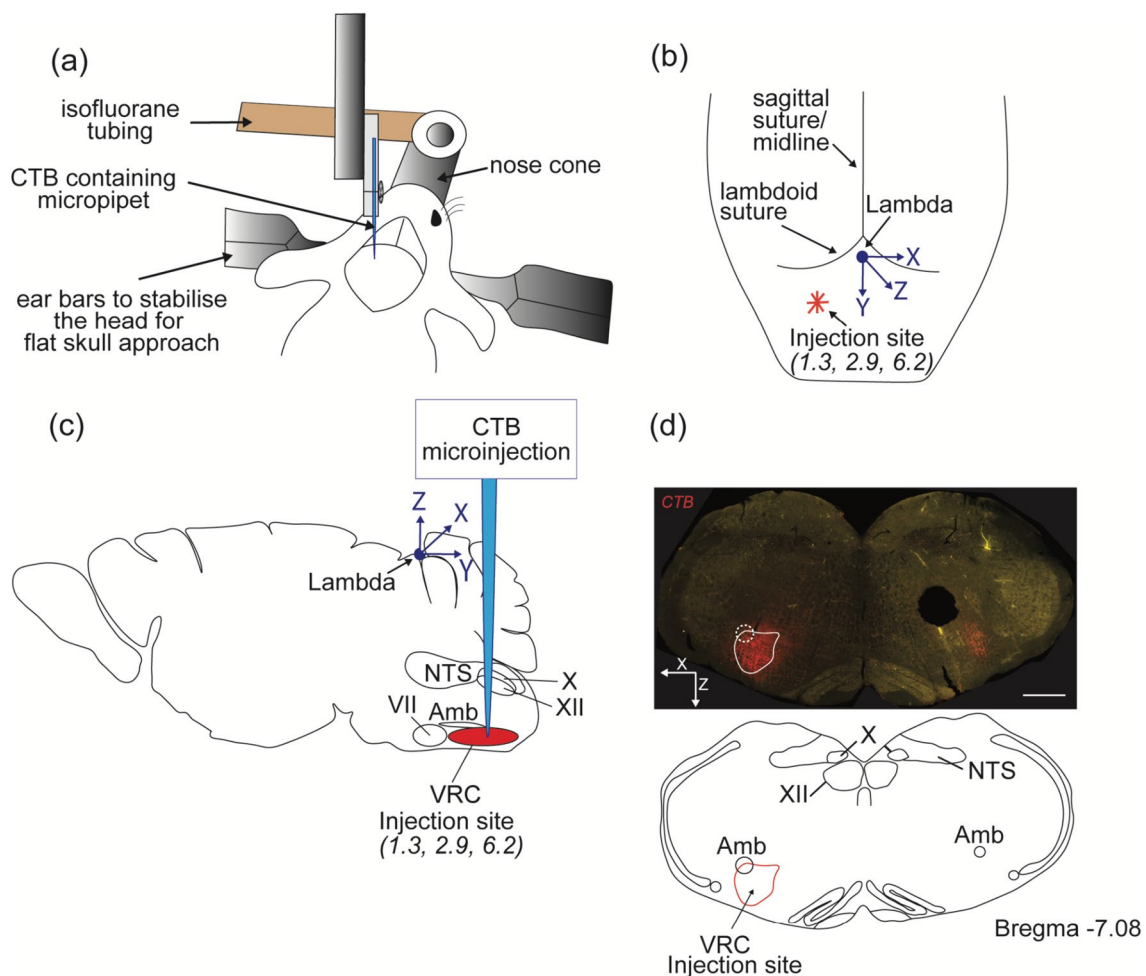


**Fig. 1** Schematic depiction of surgical approach and location of CTB injection site. **a** Mouse head mounted on the stereotaxic frame during CTB injection. The head of the mouse is positioned horizontal and symmetrical to the ear bars. There is continuous anaesthetic (isoflurane) fed to the animal through the nose cone to maintain a surgical plane of anaesthesia. **b** Schematic diagram of the frontal plane of the mouse skull indicating anatomical landmarks and stereotaxic coordinates of the injection site, which was 1.3 mm lateral to midline,

2.9 mm caudal to lambda and 6.2 mm ventral to the dorsal surface of the skull. **c** Sagittal schematic of the mouse brain indicating the location of CTB injection, the VRC, in relation to other brain areas and illustrating the anatomical trajectory of the micropipette reaching the z-coordinate. **d** A coronal brainstem image (–7.08 mm caudal to Bregma) showing an on-target CTB injection (red) in the location of the VRC, immediately ventral to the nucleus ambiguus (Amb). The scale bar is 500 µm

## Acute hypercapnia challenge paradigm

After surgical recovery, mice were randomly assigned to either room air (RA) or acute hypercapnia (AH) challenge groups. A total of ten animals with on-target injection sites were used for analysis (5 RA vs 5 AH). On the final day of the experiment, AH mice were relocated to a quiet laboratory where they were exposed to 10% CO<sub>2</sub>/90% O<sub>2</sub> in their home cages for 1 h, followed by 1 h in RA, prior to euthanasia. RA animals were treated identically, except that they breathed room air throughout the 2 h period. We used hyperoxic conditions (90% O<sub>2</sub> as previously described; Guyenet et al. 2005; Mulkey et al. 2004, 2007) for the AH challenge to minimise input from peripheral oxygen sensors (Lahiri et al. 1987), ensuring that ventilatory responses to hypercapnia were mediated by central mechanisms.

At the end of the AH challenge, animals were deeply anaesthetised with sodium pentobarbital (> 150 mg/kg, ip) and transcardially perfused with heparinised 0.1 M phosphate buffered saline (PBS) followed by 4% paraformaldehyde (PFA, Sigma-Aldrich, NSW) in 0.1 M sodium phosphate buffer. Fixed brains were vibratome-sectioned coronally (30 µm) (Leica VT1200S, Leica, Germany) and stored in cryoprotectant solution (30% RNase-free sucrose, 30% ethylene glycol, 1% polyvinylpyrrolidone in 0.1 M sodium phosphate buffer, pH 7.4) at -20 °C.

## Non-radioactive chromogenic in situ hybridisation combined with immunohistochemistry

A template cDNA library was generated by reverse transcription of total RNA isolated from mouse brain tissue (Kumar et al. 2012). In situ hybridisation (ISH) riboprobes were synthesised from cDNA which was amplified from the cDNA library using a scaled-up PCR reaction. The PCR primers used for preprogalanin (ppGal) were ggatccatttagtgacacatagaagCACCGAGAGAGCCTTGATCCTG (with SP6 RNA polymerase promoter regions attached at the 5' end, in lowercase) and gaattctaatacactactatagggagaACGATTGGCTTGAGGAGTTGG (with T7 RNA polymerase promoter regions attached at the 5' end, in lowercase). Following purification of the amplified cDNA template (Qiaquick gel extraction kit, Qiagen), riboprobes were prepared by in vitro transcription incorporating digoxigenin-11-UTP (Roche Applied Science, Mannheim, Germany) using the AmpliScribe T7 FLASH transcription kit (Epicentre Biotechnologies, Madison, WI, US) for antisense and SP6 RiboMAX large-scale RNA production system (Promega, Madison, WI, US) for sense (control).

For digoxigenin (DIG) labelled ISH, free floating brain sections (1:6 (forebrain) & 1:3 series (brainstem)) were assayed as described previously (Spirovski et al. 2012; Kumar et al. 2012). Briefly, tissue sections were incubated with DIG-incorporated riboprobes (500–1000 ng/µl) overnight at 58 °C to allow for RNA hybridisation to occur. Sections were then rinsed through a series of decreasing

**Table 1** Primary, secondary, and tertiary antibodies used in this study

Antibody	Host (mono- vs polyclonal)	Working dilution	Company (catalog no)	RRID
<b>Primary</b>				
DIG	Sheep (pc)	1:1000	Roche (11093274910)	AB_2313640
CTB	Goat (pc)	1:3000	List Biological Laboratories (703)	AB_10013220
Phox2b	Guinea pig (pc)	1:1500	Gift from Professor Hideki Enomoto (Nagashimada et al. 2012)	n/a
c-Fos	Rabbit (pc)	1:4000	Santa Cruz (sc-253)	AB_2231996
TH	Mouse	1:1000	Millipore Sigma (MAB318)	AB_2927419
TH	Sheep	1:1000	Millipore (AB1542)	AB_2927420
<b>Secondary</b>				
α-Guinea pig Cy3	Donkey	1:400	Jackson ImmunoResearch (706-165-148)	
α-Rabbit 488	Donkey	1:400	Jackson ImmunoResearch (711-545-152)	
α-Goat Cy5	Donkey	1:400	Jackson ImmunoResearch (705-175-147)	
α-mouse AMCA	Donkey	1:200	Jackson ImmunoResearch (715-155-151)	
α-Mouse biotinylated	Donkey	1:1000	Jackson ImmunoResearch (715-065-151)	
α-Sheep Cy5	Donkey	1:400	Jackson ImmunoResearch (713-175-147)	
<b>Tertiary</b>				
Extravidin Cy3		1:500	Sigma-Aldrich (E4142-1ML)	

salt concentrations and blocked prior to primary antibody incubation (24–48 h at 4 °C, antibody details are found in Table 1). Sections were rinsed with tris buffered saline (TBS) and incubated with fluorescently tagged secondary antibodies diluted in TBS containing 1% NHS and 0.1% Tween-20 at 4 °C overnight. ppGal mRNA expressing neurons were identified by detection of alkaline phosphatase activity following immersion of tissue sections in NBT/BCIP chromogenic substrate solution. Finally, sections were mounted and coverslipped with a mounting medium (Fluoroshield with DAPI or Fluoromount Aqueous Mounting Medium, Sigma, Australia).

### Antibody characterisation

Sheep alkaline phosphatase-conjugated anti-DIG recognises the DIG-conjugated UTP incorporated into the riboprobes. Immunoblot assay demonstrated no cross reactivity of this antibody with any other known substance. Mouse brain tissue sections assayed in the absence of DIG-incorporated riboprobes lacked alkaline-phosphatase staining. The distribution of DIG-labelled ppGal riboprobes accorded with previous studies (Dereli et al. 2019).

Rabbit anti-CTB targets the purified beta subunit of CTB and was previously characterised in other studies (Geerling et al. 2016). CTB is not endogenously produced in mammals. Anti-CTB staining was clearly distinguished on tissue sections at the level of the CTB injection site (Fig. 2c–f) and CTB labelling was absent in pilot studies.

Guinea-pig anti-Phox2b was a gift from Professor Hideki Enomoto (Kobe University, Kobe, Hyogo, Japan). Antigen specific immunolabeling was verified by co-expression with rabbit anti-Phox2b (gift from Professor Jean Francois Brunet, Ecole Normale Supérieure, Paris, France) and was consistent with previous reports of Phox2b expression in the adult mouse, as described previously by our group (Dereli et al. 2019). Specifically, rabbit anti-Phox2b antibody demonstrated labelling in catecholaminergic neurons and complete absence of immunoreactivity in Phox2b knockout mice (Lazarenko et al. 2009; Nagashimada et al. 2012).

Rabbit anti-c-Fos was previously characterised (Spirovski et al. 2012; Senthilkumaran et al. 2018; Fazekas et al. 2020). Western blot analyses showed that the antisera recognise Fos (62 kDa, Jurkat T lymphocyte cells), FosB, (20–60 kDa, human FosB transfected 293T lymphocyte cells), and Fra-1 and Fra-2 (23–43 kDa, human Fra-2 transfected 293T lymphocyte cells) proteins (Spirovski et al. 2012). After antibody titration, 1:4000 dilution gave specific optimum labelling with no background staining. c-Fos staining following acute hypercapnia challenge showed a staining pattern in respiratory nuclei, as previously described (Teppema et al. 1997).

Western blotting with mouse anti-tyrosine hydroxylase (TH) antibody confirmed that it specifically recognizes a 55–60 kDa protein in ventral tegmental area lysates (manufacturer's datasheet; Gumbs et al. 2019). Sheep anti-TH antibody was previously characterised by Baur et al. (2018). Western blot of rat brain corpus striatum homogenates show a single band of ~62 kDa (manufacturer's datasheet; Haycock and Haycock 1991; Kansy et al. 2004). TH immunofluorescence for both antibodies was identical to previously described data (Lazarenko et al. 2009).

### Image processing, cell counts and analysis

Slides were scanned using either a Vectra Polaris Automated Quantitative Pathology Imaging System (Perkin Elmer, Waltham, MA, USA) or Zeiss Axioimager M2 (Carl Zeiss AG, Oberkochen, Germany) at the Mark Wainwright Analytical Centre, UNSW, Sydney. Neuronal profiles were plotted using StereoInvestigator software version 9 (MicroBrightfield, USA). Tissue sections were aligned to the mouse stereotaxic brain atlas of Franklin and Paxinos (2007) (see Supplementary Information).

For qualitative analysis of neuronal profiles within a particular brain region, five sections per animal were screened. ppGal + neuronal distribution was graded as described previously (Bowman et al. 2013; Kuteeva et al. 2004; Verner et al. 2008): – (not expressed), + (scattered sparsely), ++ (expressed by < 1/3 of neurons in the area), +++ (expressed by > 1/3 of neurons in the area) (see Table 2, Supplementary Fig. 3).

For quantitative analysis, only neurons with DAPI-stained nuclei were considered for counting. Since few CTB + neurons were detected on the contralateral side (< 1/5), counts were made only from the ipsilateral side. Phox2b and TH were used to assist identification of defined neuronal populations, i.e. the RTN, NTS, LPB and KF. CTB, Phox2b, and ppGal mRNA expressing cells were counted. c-Fos + cells were only counted if they co-localised with another neuronal marker, such as CTB or ppGal. Cellular profiles were manually counted for all analyses except for the ppGal chromogenic mRNA stain in the forebrain which was counted semi-automatically using the 'positive cell detection' function in Qupath software (Bankhead et al. 2017). Total cell counts were obtained following Abercrombie correction (Abercrombie 1946): for 30 µm thick sections, an average nuclear width of  $7.2 \pm 0.2$  µm and average section thickness of  $29.7 \pm 1$  µm was measured from 30 cells per section, in 10 sections from each of 10 animals. All values are given  $\pm$  SEM values and comparisons were initially performed using two-way ANOVA. Where required, post-hoc analysis was conducted using Sidak's methods on GraphPad Prism. Representative images were first imported into Fiji



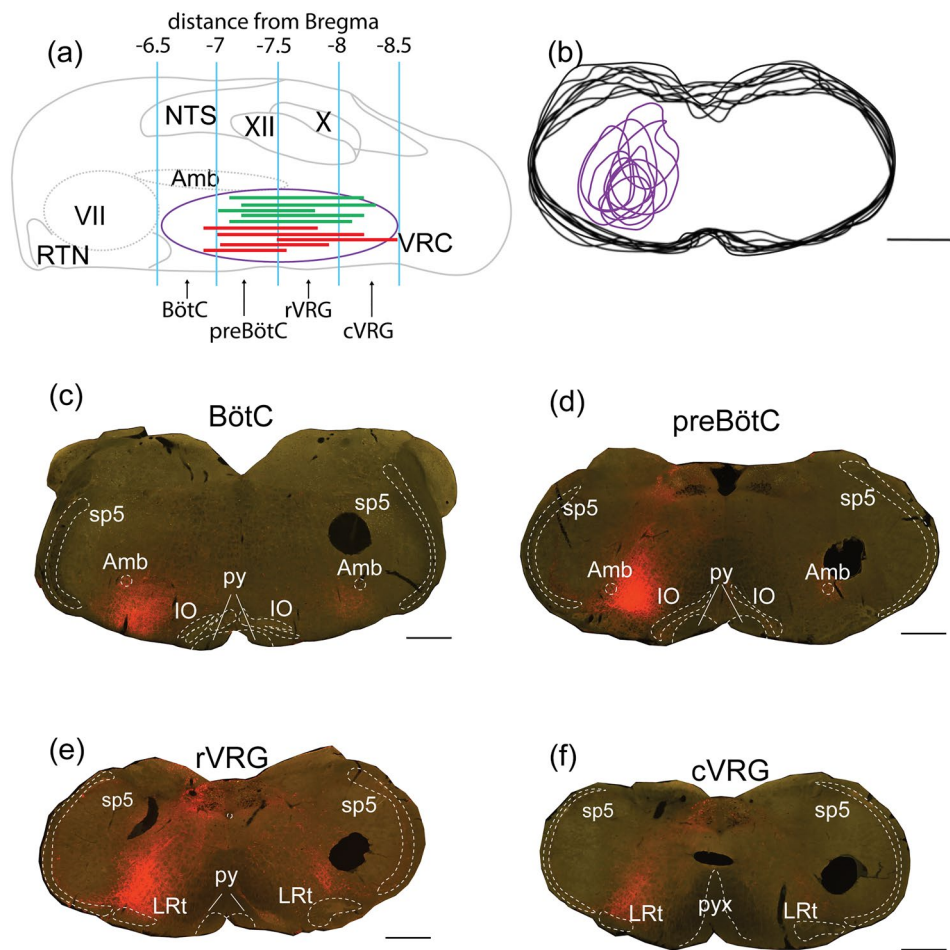


**Fig. 2** Verification of CTB injection site targeting the VRC. **a** Sagittal schematic of mouse brainstem illustrating rostral-caudal extent of the on-target injections (red and green lines) used for analysis. Each line in the VRC represents an animal: each green line represents a room air control animal; red lines represent animals that were exposed to 10% CO<sub>2</sub>, 1 h. **b** Schematic overlay of coronal sections from ten animals depicted in **(a)**, showing dorsoventral and mediolateral extent of the on-target injection sites (purple). **c–f** Representative images from an animal with an on-target injection site at four different levels of

the VRC showing CTB in red staining: **c** Bötzing complex (BötC) at Bregma  $-6.84$  mm, **d** preBötzing complex (preBötC) at Bregma  $-7.32$  mm, **e** rostral ventral respiratory group (rVRG) at Bregma  $-7.64$  mm and **f** caudal ventral respiratory group (cVRG) at Bregma  $-8$  mm. *RTN* retrotrapezoid nucleus; *VII* facial motor nucleus; *NTS* nucleus of the solitary tract; *XII* hypoglossal nucleus; *X* dorsal motor nucleus of the vagus; *Amb* nucleus ambiguus; *LRT* lateral reticular nucleus; *pyx* pyramidal decussation; *sp5* spinal trigeminal tract; *IO* inferior olive. Scale bar is 500  $\mu$ m for **b**, 1 mm for **c–f**

(RRID:SCR\_002285) as TIFF files for brightness/contrast adjustment to increase the clarity and to reflect true rendering. Images were not otherwise altered. TIFF images were then imported into CorelDraw Graphics Suite X7 (64-bit) or Adobe Illustrator CC (2019) for final presentation.

## Results

### Verification of CTB injection site targeting the VRC

Figure 2a, b summarises the locations of injection sites from experiments included in this study. We successfully targeted the VRC; CTB deposits were centred at the preBötC

and rVRG in 9/10 injections (Bregma  $-7.2$  to  $-7.7$  mm) and rVRG and cVRG in 1/10 injections (Bregma  $-6.9$  to  $-8.5$  mm) (Fig. 2a). Figure 2b illustrates the mediolateral and dorsoventral extent of the 10 CTB injections used for quantitative analysis. Figure 2c–f shows representative coronal images from an animal with an on-target injection site at four different compartments of the VRC.

### Brain nuclei that project to the VRC

Qualitative analysis (Table 2) identified 30 brain nuclei and 51 subnuclei that project to the VRC which were later quantified in Fig. 6. The majority of CTB labelled neurons were located ipsilateral to injection sites (See

**Table 2** Relative abundance and CO<sub>2</sub> responsiveness of neurons containing CTB, ppGal mRNA (*n* = 9–10)

Location	Nuclei and subnuclei	CTB +		CTB + /c-Fos +		CTB + /ppGal +	
		Ipsil	Contral	RA	AH		
Cortical	Motor cortex:						
	Primary motor cortex (M1)	+	+	+	+	–	
	Secondary motor cortex (M2)	+	+	+	+	–	
	Insular cortex:						
	Dysgranular insular cortex (DI)	+	+	+	+	–	
	Agranular insular cortex (AI)	+	+	+	+	–	
	Somatosensory cortex:						
	Primary somatosensory cortex (S1)		+	+	+	–	
	Secondary somatosensory cortex (S2)	+	+	+	+	–	
	Secondary auditory cortex (Au)	+	+	+	+	–	
	Temporal association cortex (TeA)	+	+	+	+	–	
	Ectorhinal cortex (Ect)	+	+	+	+	–	
	Perirhinal cortex (PRh)	+	+	+	+	–	
	Subcortical	Bed nucleus of stria terminalis (BNST)	++	–	+	+	+
Amygdala:							
Extended amygdala (EA)		+	–	+	–	–	
Central amygdaloid nucleus (CeA)		+++	+	++	++	+	
Medial amygdaloid nucleus (MeA)		+++	–	–	–	+	
Basolateral amygdaloid nucleus (BLA)		++	–	+	+	–	
Hypothalamus:							
Anterior hypothalamic nucleus (AHN)		+	+	+	+	+	
Lateral preoptic area (LPA)		++	–	n/a	–	+	
Median preoptic nucleus (MPA)		+	–	+	+	+	
Dorsomedial hypothalamic nucleus (DMH)		+++	+	+	+	+	
Ventromedial hypothalamic nucleus (VMH)		++	+	+	+	+	
Paraventricular hypothalamic nucleus (PVN)		++	+	+	+	+	
Lateral hypothalamic area (LHA)		+++	++	++	++	+	
Thalamus:							
Ventromedial thalamic nucleus (VM)†		+	+++	–	–	–	
Ventral posteromedial thalamic nucleus (VPM)†		+	+++	–	–	–	
Submedius thalamic nucleus (STh)†		+	++	+	+	–	
Reticular formation		+	–	–	n/a	–	
Interfascicular nucleus (IF)		+	+	–	n/a	–	
Zona incerta (ZI)		+	+	+	–	–	
Anterior pretectal nucleus (APT)		–	++	–	n/a	–	
Midbrain		Periaqueductal gray (PAG):					
		Dorsomedial periaqueductal gray (DMPAG)	++	+	–	–	–
		Ventrolateral periaqueductal gray (VLPAG)	++	+	+	+	–
		Lateral periaqueductal gray (LPAG)	+++	+	+	+	–
		Intermediate white layer of superior colliculus (SC)	–	+++	–	n/a	–
Pons	Edinger-Westphal nucleus (EW)	+++	+++	–	n/a	–	
	Lateral parabrachial nucleus (LPB)	++	+	+	+	–	
	Medial parabrachial nucleus (MPB)	++	+	+	+	–	
	Kölliker-Fuse (KF)	+++	+	+	+	–	
	Barrington's nucleus (Bar)	+	–	–	–	–	
	Pontine reticular nucleus (PnO)	+	+	–	–	–	
	Raphe magnus (RMg)	+	+	–	+	–	
	Subcoeruleus nucleus (SubC)	++	+	+	+	–	

**Table 2** (continued)

Location	Nuclei and subnuclei	CTB +		CTB +/c-Fos +		CTB +/ppGal +
		Ipsil	Contral	RA	AH	
Medulla	A5 region	++	+	-	-	-
	Intermediate reticular nucleus (IRt)	+	+	-	-	-
	Raphe pallidus (RPa)	+	+	+	++	-
	Raphe magnus (RMg)	+	+	-	+	-
	Retrotrapezoid nucleus (RTN)	++	+	+	++	+++
	Ventral respiratory column (VRC)	n/a	++	-	+	-
	Cuneate nucleus (Cu)	++	-	-	-	-
	Nucleus of the solitary tract (NTS)	+++	+	-	+	++
	Area postrema (AP)	+++	+	-	+	-
	Spinal trigeminal nucleus (Sp5)	++	-	-	-	-

All anatomical areas listed are according to the mouse stereotaxic atlas (Franklin and Paxinos 2007). For each animal, five sections per area were analysed. Refer to Supplementary Fig. 3 for the qualitative analysis scale used to grade cellular expression

- undetectable; + scattered sparsely; ++ expressed by 1/3 of the neurons in the area; +++ expressed by > 1/3 of the neurons in the area; n/a not available; AH acute hypercapnia challenge; RA room air

†Processes

Supplementary Fig. 4). In the neocortex, CTB + neurons were identified in the motor, insular, somatosensory, auditory, temporal association and rhinal cortices. Brainstem regions that contained CTB + cell bodies included the PAG, superior colliculus (SC), KF, LPB, Edinger–Westphal nucleus, Barrington’s nucleus, subcoeruleus nucleus (SubC), RTN, NTS, cuneate nucleus, trigeminal nucleus, area postrema, reticular nucleus, and VRC (Table 2).

In the amygdala, projecting neurons were identified in the extended amygdala (EA), central (CeA), medial (MeA) (Fig. 3) and basolateral amygdaloid nucleus (BLA). In the hypothalamus, VRC-projecting subnuclei were identified in the preoptic areas (Fig. 4), DMH, ventromedial hypothalamic nucleus (VMH), paraventricular hypothalamic nucleus (PVN) and lateral hypothalamic area (LHA) (Fig. 5). Quantitatively, the forebrain population with the most abundant CTB + neurons was LHA ( $168 \pm 27$ ,  $n = 10$ ), followed by MeA ( $165 \pm 30$ ,  $n = 10$ ), CeA ( $138 \pm 15$ ,  $n = 10$ ) and DMH ( $99 \pm 17$ ,  $n = 10$ ) (Fig. 6a).

There were CTB + neurons throughout the PAG, including the dorsomedial (DMPAG), lateral (LPAG) and ventrolateral compartments (VLPAG) (Fig. 7a, b). Counts between Bregma levels -4.72 and -4.48 showed an average of  $951 \pm 68$  ( $n = 7$ ) VRC projecting neurons within these compartments (Fig. 7d).

In the pons, the LPB and KF regions contained CTB + neurons throughout the entire rostrocaudal extent of each nucleus (Figs. 9a and 10a). In the KF (Bregma -5.08 and -4.84), an average of  $1082 \pm 80.6$  neurons ( $n = 7$ ) were CTB + of which 5.9% was Phox2b + ( $50 \pm 8$  total cell counts,

$n = 7$ ) (Fig. 8d). This represented 23.9% of all Phox2b + neurons in the KF area ( $346 \pm 59$  total cell counts,  $n = 7$ ). In the LPB (Bregma levels -5.44 and -5.2), there was an average of  $775 \pm 56$  ( $n = 9$ ) CTB + neurons out of which 10.5% were Phox2b + neurons ( $75 \pm 1$  total cell counts,  $n = 9$ ) (Fig. 9d).

RTN neurons are characterised to be Phox2b + (a transcription factor) and TH-, therefore counts were made from Phox2b +/TH- neurons in the parafacial region. 33.5% of RTN neurons ( $219 \pm 15$  total cell counts,  $n = 9$ ) were immunoreactive for CTB on the ipsilateral side (Fig. 10d).

In the NTS, CTB immunoreactivity was mainly observed in the caudal division (cNTS). In the rostral NTS (rNTS), defined by disappearance of the area postrema, no CTB + neurons were detected. Therefore, quantitative analysis was only performed for the cNTS (Bregma levels -8.04 and -6.84). An average of  $3420 \pm 451$  neurons ( $n = 9$ ) were CTB + and 59.9% of these neurons were Phox2b + ( $1986 \pm 248$  total cell counts,  $n = 9$ ) (Fig. 11d).

### Multiple VRC projecting neuronal populations in the forebrain express ppGal mRNA

The forebrain regions that express ppGal mRNA were identified (Table 2) and quantified (Fig. 6b). ppGal ISH product was observed in motor and insular cortices, bed nucleus of stria terminalis (BNST), CeA, MeA, anterior hypothalamic nucleus (AHN), lateral (LPA) and medial (MPA) preoptic areas, DMH, VMH, PVN, LHA and zona incerta (ZI). Amongst these, the region that contained the highest mean count of ppGal + neurons, was MPA ( $224 \pm 36$ ,  $n = 8$ ),



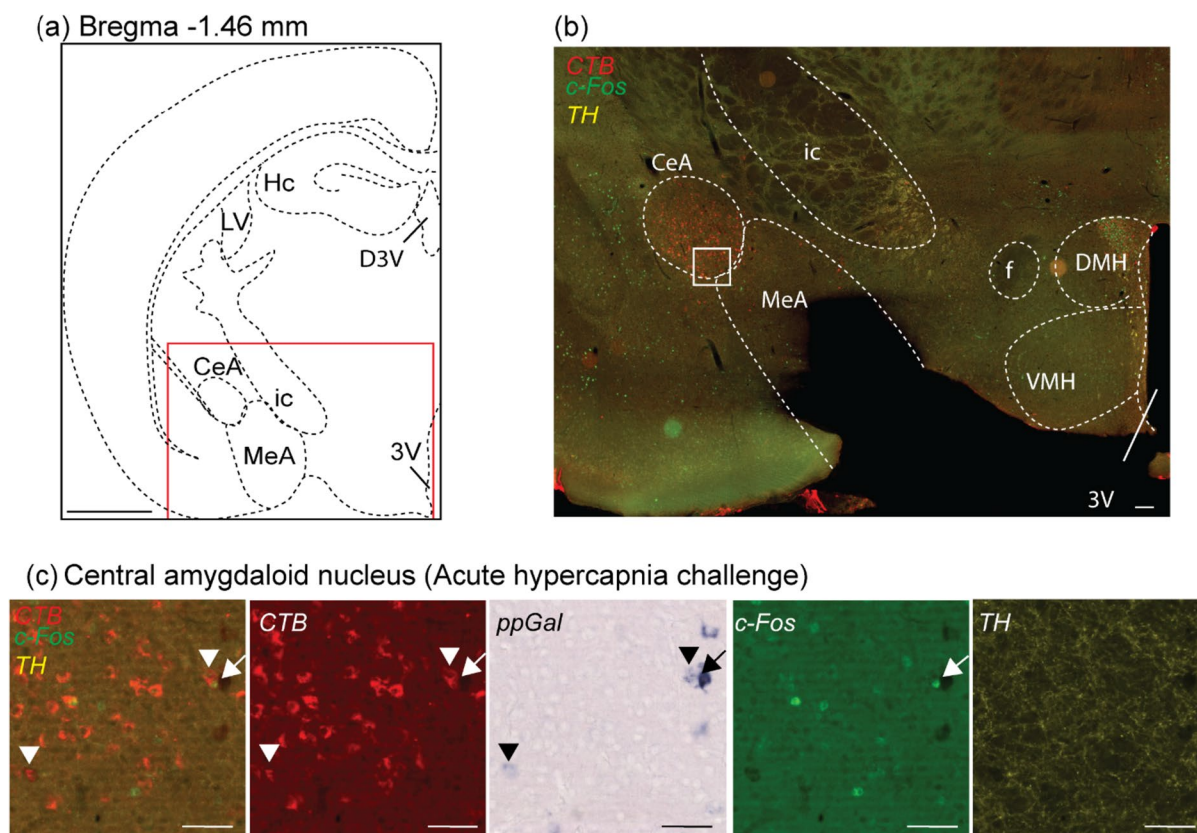


**Fig. 3** A subpopulation of central amygdaloid nucleus (CeA) neurons projected to the VRC, are galaninergic, but not c-Fos+. **a** Schematic brain hemisection corresponding to Bregma  $-1.46$  mm. The inset in **(a)** is enlarged in **(b)**, showing the relative locations of the CeA and MeA. **c** is a high magnification image of the inset in **(b)**, with CTB (red), ppGal (brightfield), c-Fos (green) and TH (yellow) labelling after acute hypercapnia challenge. Arrowheads point to VRC-project-

ing neurons that are ppGal+ and are not c-Fos+. Arrow points to a ppGal+ neuron that does not project to the VRC and is c-Fos+. Scale bars are 1 mm in **(a)**, 100  $\mu$ m in **(b)** and 50  $\mu$ m in **(c)**. Schematic diagram **(a)** is adapted from Franklin and Paxinos (2007). *ic* internal capsule; *VMH* ventromedial hypothalamic nucleus; *DMH* dorsomedial hypothalamic nucleus; *f* fornix; *3V* third ventricle; *Hc* hippocampus; *ic* internal capsule; *LV* lateral ventricle; *D3V* dorsal 3rd ventricle

followed by LPA ( $222 \pm 46$ ,  $n = 8$ ), DMH ( $139 \pm 59$ ,  $n = 10$ ) and LHA ( $132 \pm 34$ ,  $n = 10$ ).

Two regions (hypothalamus, amygdala) and 10 associated subnuclei (BNST, CeA, MeA, AHN, LPA, MPA, DMH, VMH, PVN and LHA) contained double labelled neurons that project to the VRC and express ppGal (Fig. 6c). LPA had the highest proportion of VRC-projecting neurons that express ppGal (3.6%,  $4 \pm 2.5$  total cell counts,  $n = 5$ ), followed by the LHA (3.3%,  $6.6 \pm 4.3$  total cell counts,  $n = 5$ ). The PVN and the VMH had distinct CTB+ and ppGal+ neuronal populations, but no ppGal+/CTB+ double labelled neurons were detected.

In the brainstem, only the RTN (Fig. 10a–c) and NTS (Fig. 11a–c) contained VRC projecting neurons that also express ppGal mRNA (CTB+/ppGal+). In the RTN, 31.7% ( $68 \pm 6$  total cell counts,  $n = 9$ , Fig. 10d) of CTB+ neurons were ppGal+, and in the NTS, 14.8% ( $462 \pm 42$  total cell counts,  $n = 9$ , Fig. 11d) of CTB+ neurons were ppGal+. There

was a region between the rostral KF and LPB that contained some ppGal+ neurons but none of these were CTB+.

### VRC-projecting neurons in the RTN are activated in response to the central respiratory chemoreflex, and most of these neurons are galaninergic

Typically, the basal level of c-Fos expression in the brain is low in the absence of any cellular stimuli. There was no statistically significant difference in c-Fos expression between the RA and AH groups, within VRC-projecting neurons including ppGal+ neurons for any of the forebrain regions assessed (Fig. 6d).

In the pons, 10.5% ( $88 \pm 22$ , total cell counts,  $n = 3$ ) of VRC projecting neurons in the PAG had a basal c-Fos expression in room air which did not change following AH challenge (6.7%,  $68 \pm 12$ , total cell counts,  $n = 4$ ) (Fig. 7c, e, f). While CTB+ neurons were located only in the DMPAG,

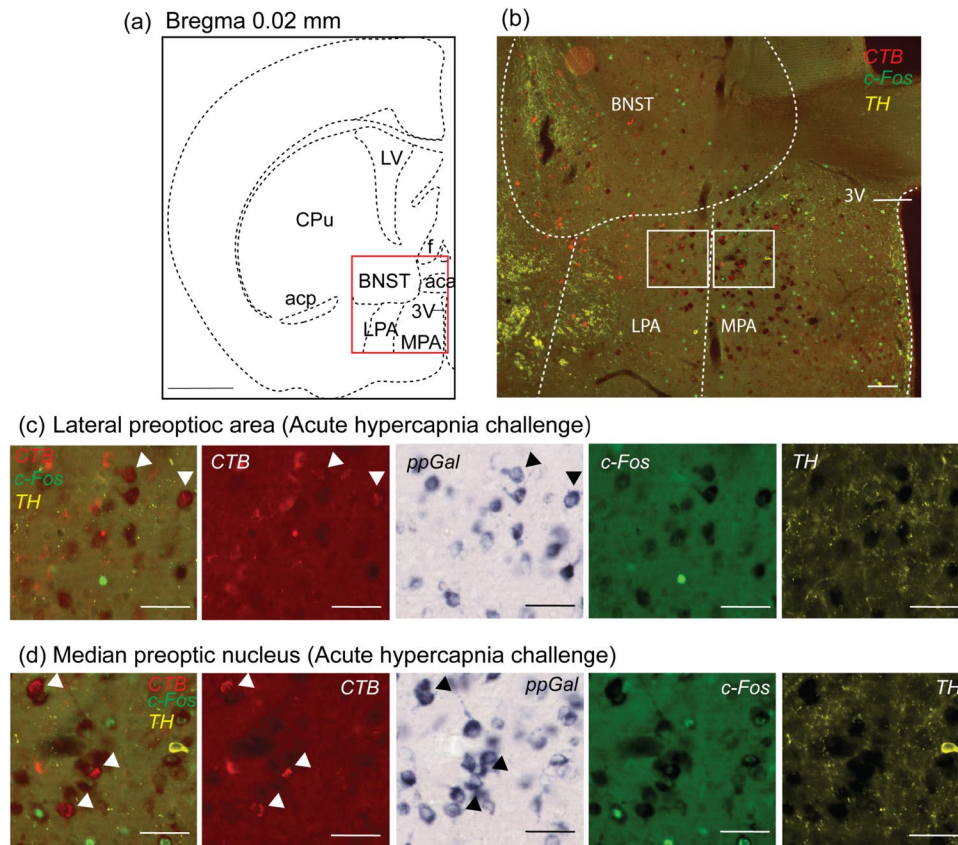


**Fig. 4** A subpopulation of VRC-projecting lateral preoptic area (LPA) and median preoptic nucleus (MPA) neurons are galanergic but not responsive to acute hypercapnia challenge. **a** Schematic of a brain section corresponding to Bregma 0.02 mm. The red box in **(a)** is depicted in **(b)** which is a representative low resolution photomicrograph of the LPA and MPA containing ppGal, CTB, c-Fos and TH labelling and major landmarks. Higher magnification of the insets in **(b)** are presented in panels **(c)** and **(d)** with CTB (red), ppGal (brightfield), c-Fos (green) and TH (yellow) labelling after acute hypercap-

nia challenge. Arrowheads point to examples of ppGal+ neurons that project to the VRC. None of the projecting ppGal+ neurons were activated following acute hypercapnia. Scale bars are 1 mm in **(a)**, 100  $\mu$ m in **(b)** and 50  $\mu$ m in **(c)** and **(d)**. Schematic diagram **(a)** is adapted from Franklin and Paxinos (2007). *BNST* bed nucleus of stria terminalis; *3V* third ventricle; *CPu* caudate putamen; *acp* anterior commissure posterior nerve; *aca* anterior commissure anterior part; *LV* lateral ventricle; *f* fornix

LPAG and VLPAG, c-Fos+ neurons were distributed across all PAG compartments.

In the KF, activation of CTB+ neurons and CTB+ / Phox2b+ subpopulation did not change from basal levels after AH challenge (3.7% vs 4.1%,  $35 \pm 4$  vs  $51 \pm 20$  total cell counts,  $n=3-4$ ) and (20.4% vs 12%,  $10 \pm 2$  vs  $15 \pm 13$  total cell counts,  $n=3-4$ ) respectively (Fig. 8c, e, f). In the KF region, CTB+ neurons were abundant in the KF core, whereas c-Fos+ and ppGal+ neurons were distributed more dorsally, the latter being positioned between the KF and LPB, and again Phox2b+ neurons were distributed more medially (Fig. 8a, b).

A similar trend was observed in the LPB; CTB positive neurons in the LPB had a basal activation of 10.9% ( $72 \pm 9$ , total cell counts,  $n=5$ ) and remained non-responsive to AH challenge (9.3%,  $83 \pm 4.2$ , total cell counts,  $n=4$ ). The projecting Phox2b+ subpopulation was not responsive to

AH challenge either; with a basal activation of 27.9% ( $24 \pm 6$ , total cell counts,  $n=5$ ) and 22.4% ( $10 \pm 4$ , total cell counts,  $n=4$ ) following AH challenge (Fig. 9c, e, f). CTB+, c-Fos+ and Phox2b+ neurons in the LPB area had a distinctive distribution with CTB+ neurons close to the dorsolateral surface followed by c-Fos+ neurons more medially and Phox2b+ neurons that appeared further medial to the superior cerebellar peduncle (Fig. 9a, b).

The proportion of chemoresponsive NTS neurons projecting to the VRC did not increase significantly following AH challenge (8.2% vs 12.4%,  $219 \pm 30$  vs  $429 \pm 32$  total cell counts,  $n=4-5$ ). Similar results were obtained for both of the Phox2b+ and ppGal+ projecting NTS subpopulations (10.1% vs 17%,  $172 \pm 36$  vs  $315 \pm 44$ , total cell counts  $n=4-5$ ) and (6.7% vs 16.9%,  $26 \pm 2$  vs  $85 \pm 29$ , total cell counts,  $n=4-5$ ) respectively (Fig. 11a-c, e-f).

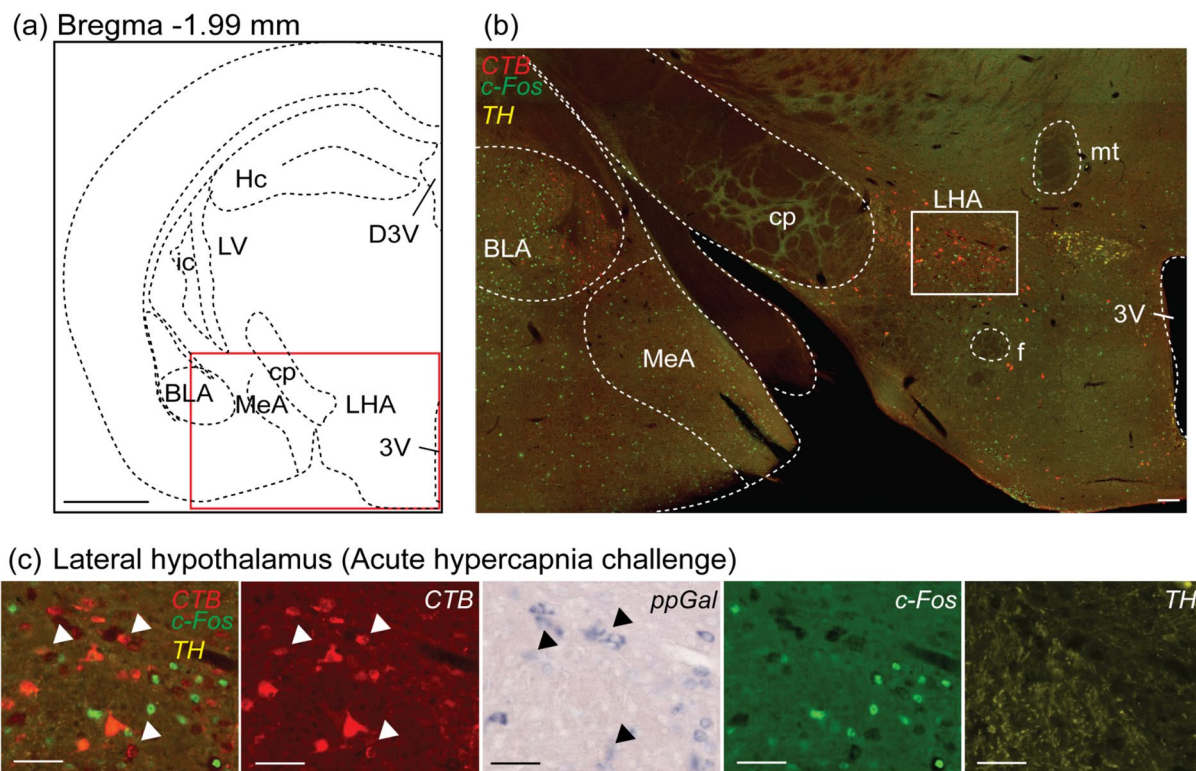


**Fig. 5** A subpopulation of VRC projecting lateral hypothalamus (LHA) neurons are galanergic but not responsive to acute hypercapnia challenge when compared to control conditions. **a** Schematic of a brain section corresponding to Bregma  $-1.99$  mm. The red box in **(a)** is the area depicted in **(b)** showing the relative location of the LHA. **(c)** is a high magnification image of the inset in **(b)**, with CTB (red), ppGal (brightfield), c-Fos (green) and TH (yellow) labelling after acute hypercapnia challenge. Arrowheads point to examples of

ppGal+neurons projecting to the VRC. None of these ppGal+neurons were activated following acute hypercapnia, although there were many c-Fos+neurons in the area. Scale bars are 1 mm in **(a)**, 100  $\mu$ m in **(b)** and 50  $\mu$ m in **(c)**. Schematic diagram **(a)** is adapted from Franklin and Paxinos (2007). BLA basolateral amygdaloid nucleus; MeA medial amygdaloid nucleus; f fornix; mt mammillothalamic tract; Hc hippocampus; cp cerebral peduncle; ic internal capsule; LV lateral ventricle; D3V dorsal 3rd ventricle

The RTN was the only region that contained VRC projecting neurons exhibiting increased c-Fos immunoreactivity in response to AH challenge. Out of all the RTN neurons projecting to the VRC, 7.8% exhibited basal activation in animals under room air conditions ( $17 \pm 6$  total cell counts,  $n = 5$ ), compared to 43.7% ( $90 \pm 5$  total cell counts,  $n = 4$ ) ( $p < 0.0001$ ) in animals exposed to AH challenge. In the ppGal+RTN subgroup projecting to the VRC, 3.1% ( $2 \pm 1$  total cell counts,  $n = 5$ ) exhibited baseline activation which increased to 54.7% ( $33 \pm 6$ , total cell counts,  $n = 4$ ) ( $p < 0.0001$ ) in response to AH challenge (Fig. 10a–c, e–f).

## Discussion

This study describes all neuronal populations that project to the VRC in the mouse brain (Fig. 12), demonstrating that the VRC receives input from an extensive array of brain regions. Highlighting the importance of peptidergic regulation of

breathing, a subset of these VRC-projecting neurons express ppGal mRNA and are chemosensitive ( $\text{CO}_2$ -stimulated). Building upon our prior finding of GalR1 mRNA expression in the BötC and preBötC (Dereli et al. 2019), this study further substantiates the potential for a role of galanin within the VRC circuitry in contributing to acute or adaptive responses to hypercapnic stimuli.

## Methodological considerations

There are some technical limitations that need to be taken into consideration. First, the VRC is positioned within a functionally heterogeneous area of the ventrolateral medulla that contains neurons related to cardiovascular, respiratory, chemosensory, metabolic and motor functions. The degree to which neurons subserving different functions are spatially segregated within this region is low, and despite using a relatively small volume of CTB (20 nl), CTB deposition sites encompass multiple autonomic



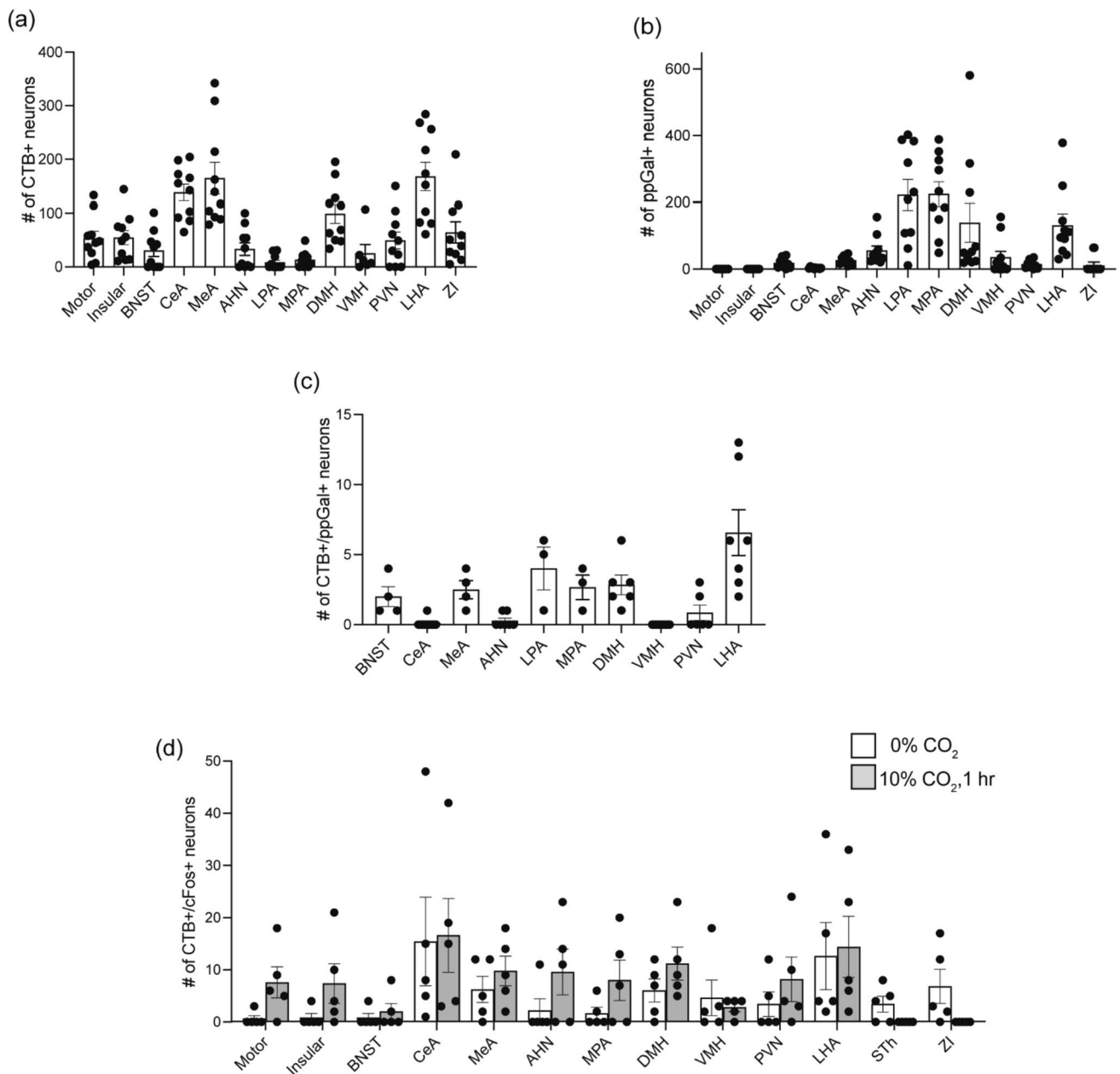


**Fig. 6** Neural populations in the forebrain that project to the VRC, including a galanergic subset, are not activated by acute hypercapnia challenge. **a** Total number of VRC-projecting (CTB+) neurons across different neural populations in the forebrain. **b** Total number of ppGal+ neurons across different neural populations in the forebrain. **c** Number of VRC projecting (CTB+) neurons that are double

labelled with ppGal. **d** Comparison of the VRC-projecting and activated (CTB+, c-Fos+ double labelled) neuronal counts between the room air and acute hypercapnia groups [two-way ANOVA, Sidak's post-hoc test:  $p > 0.05$  for all multiple comparisons, not significant, ( $n = 5$ )]. All values are given  $\pm$  SEM values. No less than six sections per area per animal was analysed

nuclei, including multiple VRC compartments. Furthermore, CTB can be taken up by fibres of passage that traverse the injection site (Saleeba et al. 2019): as a result, CTB-labelled neurons likely denote a projection to the injection site, with the caveat that their post-synaptic targets may include both respiratory and non-respiratory populations. In the future, employing retrograde viral vectors

such as AAV or rabies designed to target specific neuronal populations would overcome this problem.

### Neuronal inputs to the VRC

In total there were 30 brain nuclei including 51 subnuclei projecting to the VRC, some of which were identified in

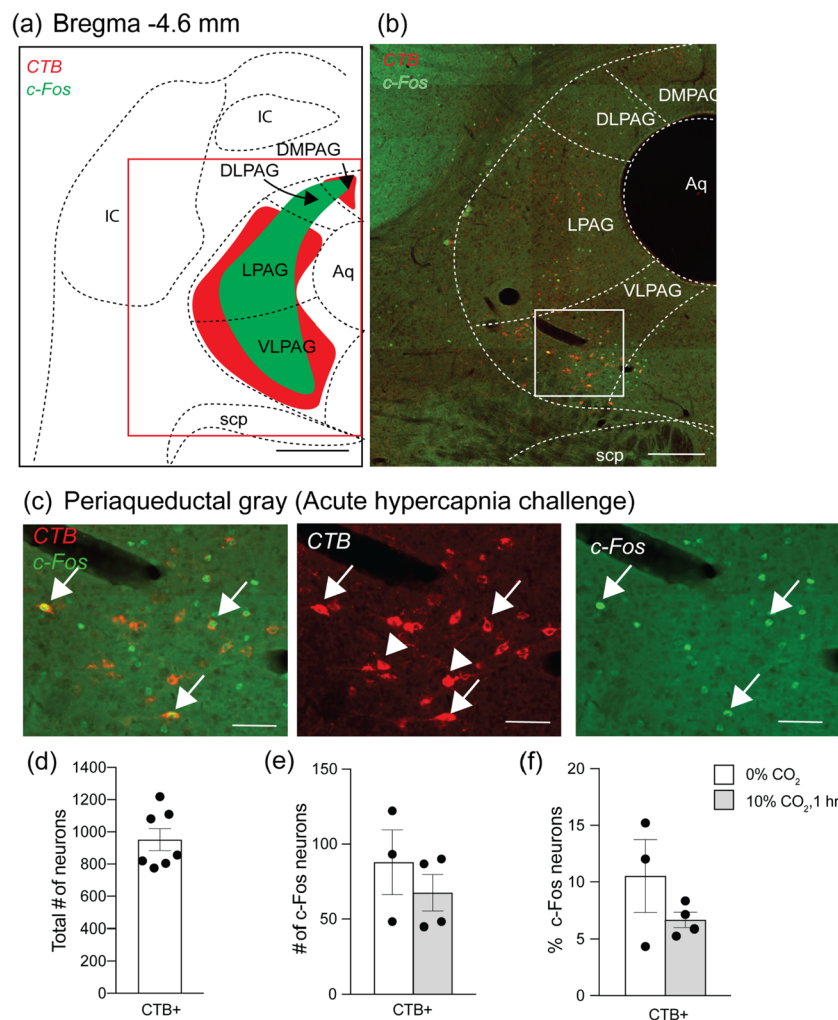


**Fig. 7** The periaqueductal gray (PAG) neurons project to the VRC but are not activated by acute hypercapnia challenge when compared to control conditions. **a** Schematic of a brain section corresponding to Bregma -4.6 mm. The red box in **(a)** is the area depicted in **(b)** which shows the relative location of the PAG. VRC projecting neurons (red) were mainly distributed in dorsomedial, lateral and ventrolateral subnuclei of the PAG (DMPAG, LPAG and VLPAG respectively). **(c)** is the higher magnification image of the inset in **(b)** with CTB (red) and c-Fos (green) labelling after AH challenge. Arrow-

heads point to examples of PAG neurons projecting to the VRC that are not c-Fos+ and arrows point to VRC projecting PAG neurons that are c-Fos+. **d** Total VRC projecting PAG neurons. **e** Total projecting PAG neurons that are activated (c-Fos+) following acute hypercapnia challenge. **f** Percentage projecting PAG neurons that are activated following acute hypercapnia challenge ( $n=3-4$ ) (two-way ANOVA:  $p<0.05$ ). **(a)** is adapted from Franklin and Paxinos (2007). Scale bars are 500  $\mu\text{m}$  in **(a)** 200  $\mu\text{m}$  in **(b)** and 50  $\mu\text{m}$  in **(c)**. IC inferior colliculus; scp superior cerebellar peduncle; Aq aqueduct

previous studies; these include the raphe nuclei (Morinaga et al. 2019; Ribas-Salgueiro et al. 2005), RTN (Rosin et al. 2006; Weston et al. 2004), PVN (Kc et al. 2002; Mack et al. 2007), NTS (Alheid et al. 2011; Ellenberger and Feldman 1990; Geerling and Loewy 2006; Nunez-Abades et al. 1993; Otake et al. 1992; Rinaman 2010), SC (Kaneshige et al. 2018) and pontine respiratory group (Ezure and Tanaka 2006; Gang et al. 1995). Our study additionally identified the following populations to have inputs to the VRC: motor, insular, sensory cortex areas, lateral and medial preoptic areas, amygdaloid regions (extended, central, medial, basomedial and basolateral),

hypothalamic areas (dorsomedial and lateral), BNST, reticular formation, interfascicular nucleus, anterior pretectal nucleus, PAG (DMPAG, VLPAG, LPAG), Pre-Edinger-Westphal nucleus, Barrington's nucleus, A5 region, SubC, cuneate nucleus and trigeminal nucleus.

The current study sought to identify the VRC projecting neuronal populations that are activated by acute hypercapnia, indicating their role in  $\text{CO}_2$ -stimulated breathing. Our findings revealed that amongst the various CTB+ brain regions, only RTN neurons displayed a significant increase in c-Fos immunolabeling following exposure to hypercapnia. This



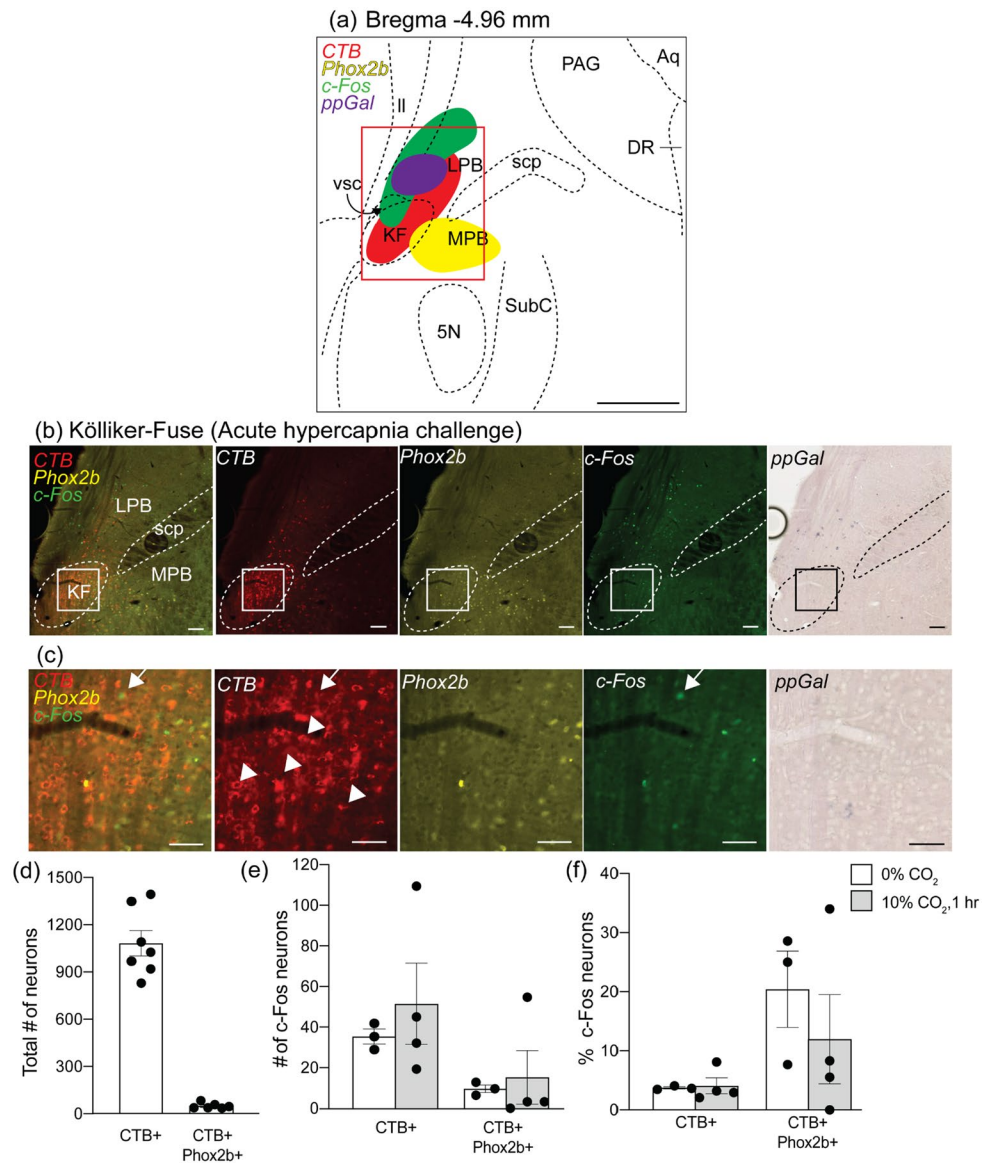


**Fig. 8** The Kölliker–Fuse (KF) neurons project to the VRC but were not ppGal+ or activated by acute hypercapnia challenge when compared to control conditions. **a** Schematic of a brainstem section corresponding to Bregma  $-4.96$  mm depicting the observed pattern of neurons expressing Phox2b (yellow), ppGal mRNA (brightfield), CTB (red) and c-Fos (green). The red box in **(a)** is enlarged in **(b)** which represents the KF region from an animal following acute hypercapnia challenge. The inset in **(b)** is magnified in **(c)** and corresponds to the core of the KF dorsoventrally. Arrowheads point to examples of KF neurons that project to the VRC and are not c-Fos+ whereas arrows point to VRC projecting KF neurons that are c-Fos+. None of the CTB+ neurons were galaninergic and very few were activated. **d** The total number of VRC projecting and VRC pro-

jecting Phox2b+KF neurons within the ipsilateral brain. **e** The total number of VRC projecting and VRC projecting Phox2b+KF neurons that are activated (c-Fos+) following acute hypercapnia challenge within the ipsilateral brain. **f** Percentage of VRC projecting and VRC projecting Phox2b+KF neurons that are activated following acute hypercapnia challenge. ( $n=3-4$ ) (two-way ANOVA:  $p>0.05$ ). **(a)** is adapted from Franklin and Paxinos (2007). Scale bars are  $500\ \mu\text{m}$  in **(a)**,  $100\ \mu\text{m}$  in **(b)** and **(c)**,  $50\ \mu\text{m}$  in **(d)** and **(e)**. MPB medial parabrachial nucleus; scp superior cerebellar peduncle; vsc ventral spinocerebellar tract; ll lateral lemniscus; PAG periaqueductal gray; DR dorsal raphe; 5N motor trigeminal nucleus; SubC subcoeruleus nucleus; Aq aqueduct

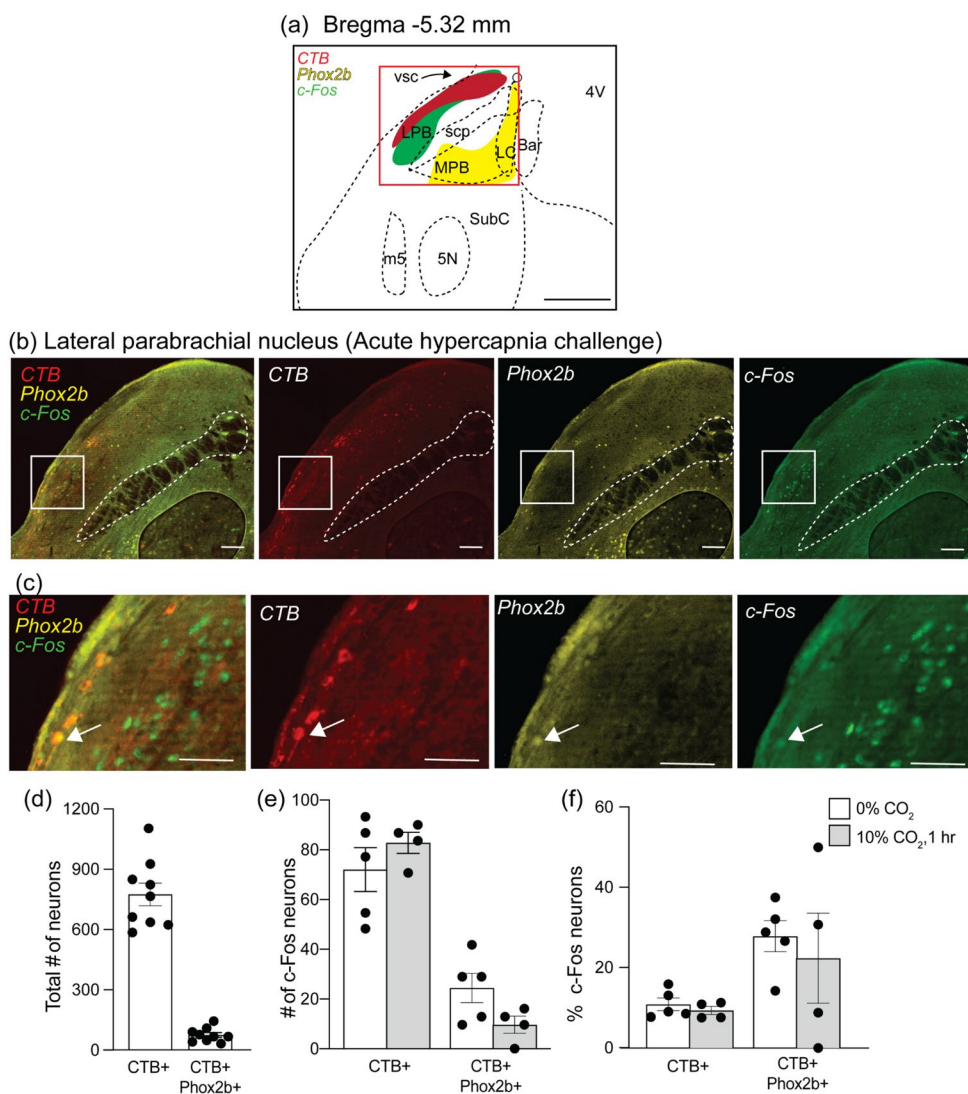


**Fig. 9** The lateral parabrachial nucleus (LPB) contains neurons that project to the VRC but were not ppGal+ or activated by acute hypercapnia challenge when compared to control conditions. **a** Schematic of a brain section corresponding to Bregma  $-5.32$  mm. Distinct populations of neurons expressing Phox2b (yellow), CTB (red) and c-Fos (green) were observed. The red box in (a) is the area depicted in (b) which is a representative image following acute hypercapnia challenge. (c) is a high magnification image of the inset in (b). The arrow points to an example of Phox2b+LPB neuron that projects to the VRC and is c-Fos+. **d** Total VRC projecting and VRC projecting Phox2b+LPB neurons within the ipsilateral brain. **e** Total VRC projecting and VRC projecting

Phox2b+LPB neurons that are activated (c-Fos+) following acute hypercapnia challenge within the ipsilateral brain. **f** Percentage VRC projecting and VRC projecting Phox2b+LPB neurons that are activated following acute hypercapnia challenge ( $n=4-5$ ) (two-way ANOVA:  $p>0.05$ ). **a** is adapted from Franklin and Paxinos (2007). Scale bars are  $500\ \mu\text{m}$  in (a),  $100\ \mu\text{m}$  in (b),  $50\ \mu\text{m}$  in (c). MPB medial parabrachial nucleus; scp superior cerebellar peduncle; vsc ventral spinocerebellar tract; m5 motor root of the trigeminal nerve; 5N motor trigeminal nucleus; SubC subcoeruleus nucleus; 4V fourth ventricle; LC locus coeruleus; Bar Barrington's nucleus

finding sheds light on how the RTN-VRC network operates and also highlights the critical role of the RTN in sensing changes in breathing due to chemical stimuli. Although not responsive to hypercapnia, other VRC-projecting neuronal populations identified in this study are known to have functional contributions to the control of breathing such as the primary motor cortex, SubC, LPB, KF and BNST. Previous studies show that inputs from the motor cortex underlie the

voluntary control of respiration (Ozaki and Kurata 2015) and orchestrate tongue movement to allow speech and swallowing (Pouget et al. 2018; Sawczuk and Mosier 2001). Similarly, in newborn mice and sheep, the SubC demonstrates increased activation (c-Fos immunoreactivity) following hypoxia (Joubert et al. 2016; Nitsos and Walker 1999). Pharmacological inhibition and electrical stimulation experiments suggest that A5 neurons modulate the respiratory response evoked from

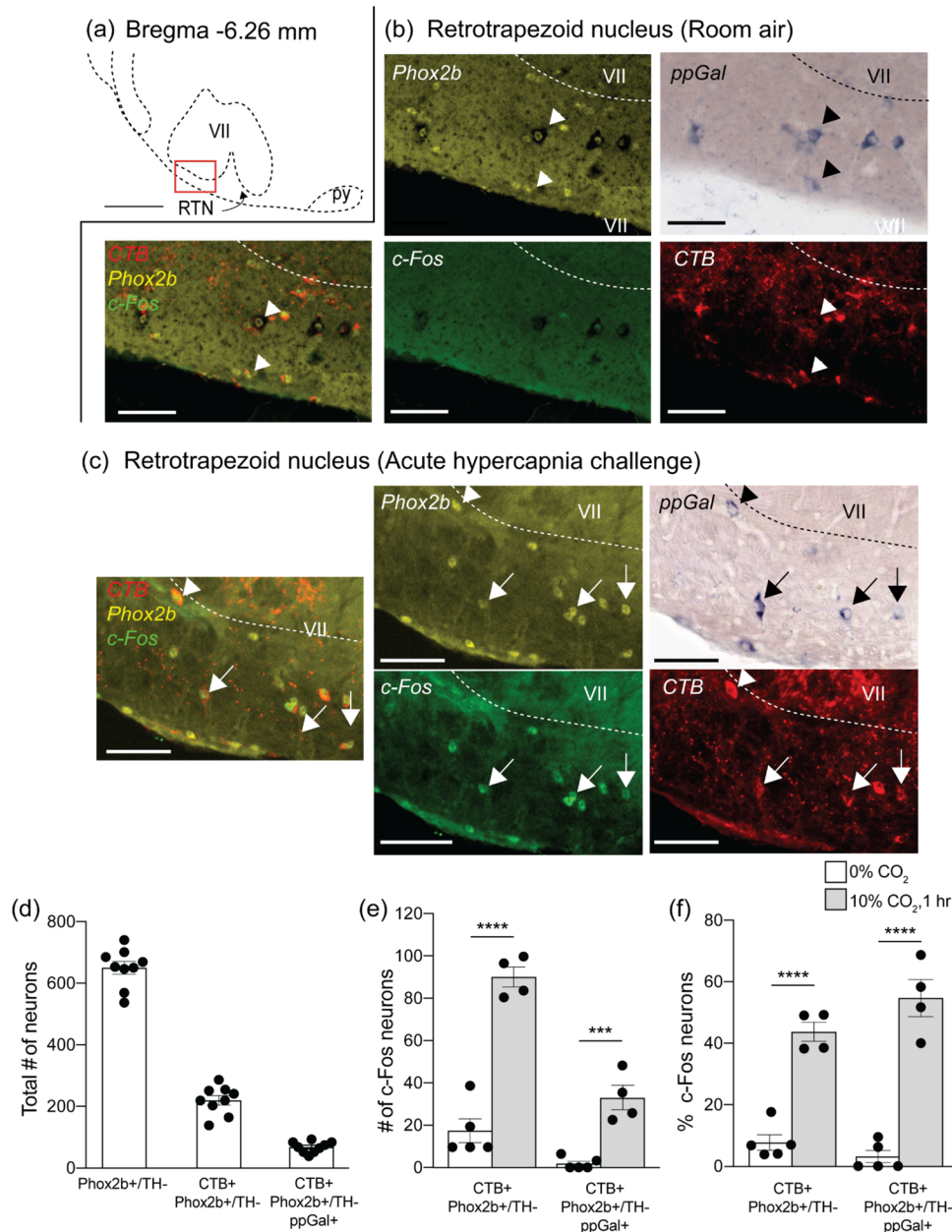


**Fig. 10** The retrotrapezoid nucleus (RTN) contains ppGal + VRC projecting neurons that are activated by acute hypercapnia challenge. **a** Schematic of the ipsilateral side of a brainstem section corresponding to Bregma  $-6.26$  mm. The red box in **(a)** is the area depicted in **(b)** and **(c)** which are representative images of the RTN region immunostained for Phox2b (yellow), ppGal mRNA (brightfield), CTB (red) and c-Fos (green) following **(b)** room air and **(c)** acute hypercapnia challenge. Arrowheads point to examples of galaninergic RTN neurons that project to the VRC but are not c-Fos+. Arrows point to ppGal+VRC projecting neurons that are c-Fos+. **d** Total RTN (Phox2b+/TH-)

neurons, VRC projecting RTN (CTB+) neurons and VRC projecting galaninergic RTN neurons within the ipsilateral brainstem. **e** Total VRC projecting RTN neurons and galaninergic RTN neurons that are activated (c-Fos+) following acute hypercapnia challenge within the ipsilateral brainstem. **f** The percentage of VRC projecting RTN neurons and galaninergic RTN neurons that are activated following acute hypercapnia challenge ( $n=4-5$ ) (two-way ANOVA:  $p < 0.05$ , Sidak's post-hoc test: \*\*\* $p < 0.001$ , \*\*\*\* $p < 0.0001$ ). **(a)** is adapted from Franklin and Paxinos (2007). Scale bars are  $500 \mu\text{m}$  in **(a)**,  $50 \mu\text{m}$  in **(b)** and **(c)**. VII facial motor nucleus; py pyramid

the PB and KF neurons (Dawid Milner et al. 2003). Furthermore, the discharge pattern of BNST neurons in cats suggests that these neurons contribute to the inspiratory onset of the respiratory cycle (Terreberry et al. 1995). Neuronal circuitry

underlying these functions was previously not clear. By identifying VRC projecting neurons in these neuronal populations, this study supports previous functional findings and contributes to a deeper understanding of the established literature.



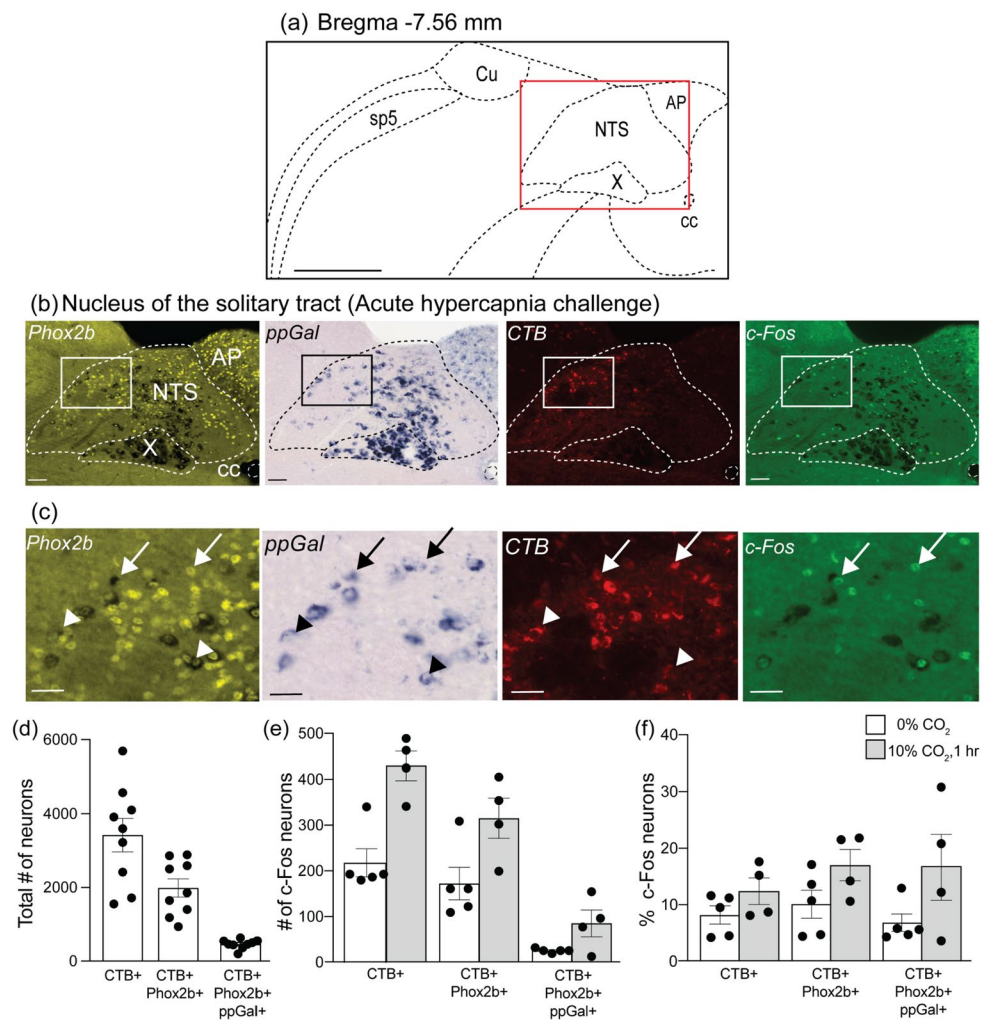


**Fig. 11** The nucleus of the solitary tract (NTS) contains galaninergic neurons projecting to the VRC (ipsilateral to the injection site); however these are not activated by acute hypercapnia challenge when compared to control conditions. **a** Coronal brainstem schematic corresponding to Bregma  $-7.56$  mm. The red box in **(a)** is the area depicted in **(b)** which is a representative low resolution photomicrograph of the caudal NTS containing Phox2b (yellow), ppGal (brightfield), CTB (red) and c-Fos (green) staining and major landmarks. Higher magnification of the insets in **(b)** are presented in panel **(c)**. Arrowheads point to examples of NTS neurons that project to the VRC and are ppGal+ but not c-Fos+ and arrows point to examples of ppGal+NTS neurons that project to the VRC and are c-Fos+.

### Galaninergic projections to the VRC

This study identified multiple brain sites that provide convergent galaninergic inputs to the VRC, suggesting that the galanin-related respiratory adaptation could be mediated by diverse inputs that may, depending on the context, be working independently or in parallel.

In the hypothalamus, LPA and MPA neurons provided small numbers of galaninergic inputs to the VRC. Optogenetic studies show that galaninergic MPA neurons govern

**d** Total number of ipsilateral cNTS neurons that project to the VRC (CTB+) and the proportion that are also Phox2b+ or ppGal+. **e** Total VRC projecting, Phox2b+ and galaninergic cNTS neurons that are activated (c-Fos+) following acute hypercapnia challenge within the ipsilateral hemisphere. **f** Percentage of VRC projecting, Phox2b+ and galaninergic cNTS neurons that are activated following acute hypercapnia challenge. ( $n=4-5$ ) (two-way ANOVA:  $p>0.05$ ). **(a)** is adapted from Franklin and Paxinos (2007). Scale bars are  $500\ \mu\text{m}$  in **(a)**,  $50\ \mu\text{m}$  in **(b)** and  $25\ \mu\text{m}$  in **(c)**. AP area postrema; X dorsal motor nucleus of the vagus; sp5 spinal trigeminal tract; Cu cuneate nucleus; cc central canal

parenting behaviour in mice (Kohl et al. 2018; Wu et al. 2014); their involvement in the regulation of breathing has not yet been established. Here, preoptic area subdivisions did not exhibit notable c-Fos immunoreactivity following chemoreflex challenge; this suggests that this area is unlikely to be involved in chemoreflex-mediated respiratory effects, although a role for the preoptic area in driving respiratory activity in response to hyperthermia has previously been described (Boden et al. 2000). Furthermore, preoptic inputs have recently been implicated in plastic changes to

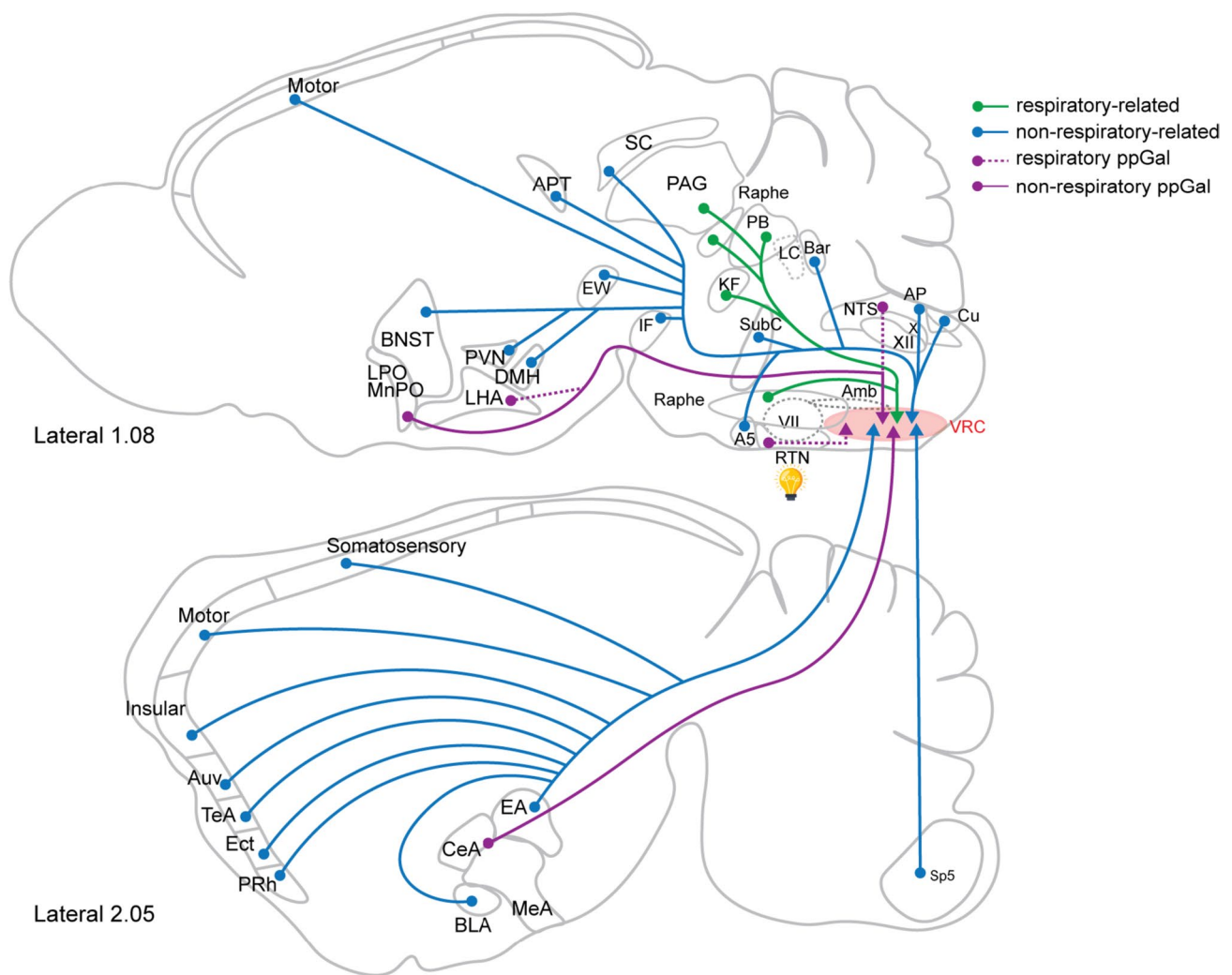


**Fig. 12** Sagittal schematic diagrams of mouse brain sections at two different lateral levels showing brain sites that provide inputs to the VRC. Green arrows indicate respiratory related, blue arrows indicate non-respiratory-related, purple arrows indicate galanergic, dashed

purple arrows indicate respiratory-related galanergic projections to the VRC. Only RTN projections, including galanergic subset, were hypercapnia activated (light bulb). See Table 2 for abbreviations

sympathetic output evoked by chronic intermittent hypoxia (Marciante et al. 2020), and therefore the identification of galanergic projections from the preoptic area to the VRC supports the involvement of this region in the control of breathing.

In this study, the LHA was another hypothalamic region identified to have inputs to the VRC from a sparse number of galanergic neurons. The LHA has orexinergic projections to the preBötC, but this represents only 2.9% of all the orexin-containing neurons in the area (Young et al. 2005). Galanergic projections from the LHA to the VRC represent a similar proportion of neurons (3.3%). Focal acidification experiments have reported some innate chemosensitivity of the LHA (Li et al. 2013), however we observed no induction of c-Fos in CTB-labelled LHA neurons and

conclude that LHA neurons that project to the VRC are unlikely to contribute to CO<sub>2</sub>-chemosensitivity.

In the amygdala, CTB-immunoreactive cell bodies were detected in the extended amygdaloid nuclei, CeA, MeA, basomedial and basolateral amygdaloid nuclei. None of these areas were associated with c-Fos induction after hypercapnia, and only the CeA and MeA contain galanergic neurons, consistent with previous studies (Kuteeva et al. 2004), of which only a small number provide input to the VRC. Deep electrode stimulation of the MeA induces apnoea in temporal lobe epilepsy patients (Nobis et al. 2018) and contributes to blunted CO<sub>2</sub> responsiveness during neonatal maternal separation (Tenorio-Lopes et al. 2017). Similarly, electrical stimulation of the CeA evokes phrenic nerve



discharge in rabbits (Cox et al. 1987). These studies provide evidence that CeA and MeA are involved in the regulation of breathing and, due to the proximity of these areas, electrical stimulation probably activates both subdivisions. Nevertheless, based on the findings of the current study, it seems unlikely that galaninergic CeA/MeA-VRC circuitry contributes to these effects.

Many studies have established that respiratory chemoreceptor populations in the NTS project to the VRC (Alheid et al. 2011; Ellenberger and Feldman 1990; Geerling and Loewy 2006; Nunez-Abades et al. 1993; Otake et al. 1992; Rinaman 2010). This study shows that a subgroup (~15%) of NTS projections to the VRC contains ppGal mRNA. However, neither VRC projecting NTS neurons overall nor the galaninergic NTS neurons demonstrated c-Fos immunoreactivity in response to hyperoxic hypercapnia, when compared to baseline c-Fos immunoreactivity. In addition to peripheral chemoreceptors that are highly sensitive to hypoxia, rather than hypercapnia, glutamatergic NTS neurons have previously been demonstrated to be hypoxia-sensitive (Takakura et al. 2006; Kline et al. 2010). Whether the galaninergic subpopulation of VRC projecting NTS neurons are hypoxia-activated remains to be determined.

The RTN has well-established projections to all subdivisions of the VRC (Rosin et al. 2006). This study demonstrates that ~44% of VRC-projecting RTN neurons are CO<sub>2</sub>-responsive. Furthermore, an anterograde tracer study has shown galanin immunoreactive boutons on VRC neurons arising from RTN neurons (Bochorishvili et al. 2012). Overall, ~32% of VRC-projecting RTN neurons (~70 neurons unilaterally) contained ppGal mRNA and ~55% of these galaninergic projections were chemoresponsive. Out of all brain regions that project to the VRC, only the galaninergic RTN subset demonstrated significant neuronal activation in response to AH challenge, when compared to room air. This highlights the crucial role of the RTN chemoreceptors, and in particular the galaninergic subpopulation, in CO<sub>2</sub>-stimulated drive to breathing, via direct innervation of VRC neurons.

In conclusion, this study reveals the brain-wide distribution of inputs to the VRC of the mouse. 12 out of 51 VRC-projecting subnuclei were galaninergic; these were the BNST, CeA, MeA, AHN, LPA, MPA, DMH, VMH, PVN, LHA, RTN and NTS. All 12 regions also contained non-galaninergic projections, the neurochemistry of which remains unidentified. We surveyed the extent to which VRC-projecting neurons are activated by acute hypercapnic stimuli and found that only VRC-projecting neurons in the RTN are both galaninergic and activated in response to hypercapnia. Together these results highlight the importance of this RTN-VRC galaninergic circuitry in central respiratory chemoreflex function by showcasing control of breathing under hypercapnic conditions via galaninergic neurons.

Further work investigating other VRC projecting areas is required to examine the circumstances under which they are functionally active, their specific neurochemistry and post-synaptic targets of all these projections.

**Supplementary Information** The online version contains supplementary material available at <https://doi.org/10.1007/s00429-024-02782-8>.

**Acknowledgements** We owe special thanks to Molecular Neuroscience Lab members from the Department of Pharmacology, UNSW Sydney. We thank Prof. Hideki Enomoto for providing us with the guinea pig anti-Phox2b antibody and Dr Anita Turner, for her expertise in rodent microsurgery. We thank the Katharina Gaus Light Microscopy Facility, Mark Wainwright Analytical Centre, UNSW Sydney for assistance in imaging.

**Author contributions** Natasha N Kumar conceptualized and supervised the research. Ayse S Dereli, Simon McMullan and Alice YS Oh conducted experiments. Ayse S Dereli and Alice YS Oh quantified and analyzed data. Natasha N Kumar and Ayse S Dereli interpreted experimental data. Ayse S Dereli prepared the figures and drafted the first version of the manuscript and all authors commented on subsequent versions of the manuscript. All authors read and approved the final manuscript.

**Funding** Open Access funding enabled and organized by CAUL and its Member Institutions. This work was supported by the Australian Research Council Discovery Project (grant no. DP180101890); Rebecca L. Cooper Medical Research Foundation (grant no. PG2018110).

**Data availability** The datasets generated during and/or analysed during the current study are available from the corresponding author on reasonable request.

## Declarations

**Conflict of interest** The authors declare no conflicts of interest. The authors have no relevant financial or non-financial interests to disclose.

**Ethical approval** Experiments were performed on adult male wild type (C57BL6/J) mice, reviewed and approved by the animal ethics committees of UNSW Sydney (ACEC 19/98A) and Macquarie University (ACEC 2018-024), in accordance with the Australian Code for the Care and Use of Animals for Scientific Purposes (National Health and Medical Research Council of Australia).

**Consent to participate** Not applicable.

**Consent to publish** Not applicable.

**Open Access** This article is licensed under a Creative Commons Attribution 4.0 International License, which permits use, sharing, adaptation, distribution and reproduction in any medium or format, as long as you give appropriate credit to the original author(s) and the source, provide a link to the Creative Commons licence, and indicate if changes were made. The images or other third party material in this article are included in the article's Creative Commons licence, unless indicated otherwise in a credit line to the material. If material is not included in the article's Creative Commons licence and your intended use is not permitted by statutory regulation or exceeds the permitted use, you will need to obtain permission directly from the copyright holder. To view a copy of this licence, visit <http://creativecommons.org/licenses/by/4.0/>.

## References

- Abbott SB, Burke PG, Pilowsky PM (2009) Galanin microinjection into the preBotzinger or the Botzinger complex terminates central inspiratory activity and reduces responses to hypoxia and hypercapnia in rat. *Respir Physiol Neurobiol* 167(3):299–306. <https://doi.org/10.1016/j.resp.2009.06.003>
- Abercrombie M (1946) Estimation of nuclear population from microtome sections. *Anat Rec* 94:239–247. <https://doi.org/10.1002/ar.1090940210>
- Alheid GF, Jiao W, McCrimmon DR (2011) Caudal nuclei of the rat nucleus of the solitary tract differentially innervate respiratory compartments within the ventrolateral medulla. *Neuroscience* 190:207–227. <https://doi.org/10.1016/j.neuroscience.2011.06.005>
- Bankhead P, Loughrey MB, Fernández JA, Dombrowski Y, McArt DG, Dunne PD, McQuaid S, Gray RT, Murray LJ, Coleman HG, James JA, Salto-Tellez M, Hamilton PW (2017) QuPath: open source software for digital pathology image analysis. *Sci Rep* 7(1):16878. <https://doi.org/10.1038/s41598-017-17204-5>
- Baur K, Hach A, Bernardi RE, Spanagel R, Bading H, Bengtson CP (2018) c-Fos marking of identified midbrain neurons coactive after nicotine administration in-vivo. *J Comp Neurol* 526(13):2019–2031. <https://doi.org/10.1002/cne.24471>
- Bochorishvili G, Stornetta RL, Coates MB, Guyenet PG (2012) Pre-Botzinger complex receives glutamatergic innervation from galaninergic and other retrotrapezoid nucleus neurons. *J Comp Neurol* 520(5):1047–1061. <https://doi.org/10.1002/cne.22769>
- Boden AG, Harris MC, Parkes MJ (2000) The preoptic area in the hypothalamus is the source of the additional respiratory drive at raised body temperature in anaesthetised rats. *Exp Physiol* 85(5):527–537. <https://doi.org/10.1111/j.1469-445X.2000.02053.x>
- Bowman BR, Kumar NN, Hassan SF, McMullan S, Goodchild AK (2013) Brain sources of inhibitory input to the rat rostral ventrolateral medulla. *J Comp Neurol* 521(1):213–232. <https://doi.org/10.1002/cne.23175>
- Burgraff NJ, Neumueller SE, Buchholz K, Langer TM 3rd, Hodges MR, Pan L, Forster HV (2018) Ventilatory and integrated physiological responses to chronic hypercapnia in goats. *J Physiol* 596(22):5343–5363. <https://doi.org/10.1113/JP276666>
- Burke PG, Abbott SB, McMullan S, Goodchild AK, Pilowsky PM (2010) Somatostatin selectively ablates post-inspiratory activity after injection into the Bötzing complex. *Neuroscience* 167(2):528–539. <https://doi.org/10.1016/j.neuroscience.2010.01.065>
- Busselberg D, Bischoff AM, Paton JF, Richter DW (2001) Reorganisation of respiratory network activity after loss of glycinergic inhibition. *Pflugers Arch* 441(4):444–449. <https://doi.org/10.1007/s004240000453>
- Cox GE, Jordan D, Paton JF, Spyer KM, Wood LM (1987) Cardiovascular and phrenic nerve responses to stimulation of the amygdala central nucleus in the anaesthetized rabbit. *J Physiol* 389:541–556. <https://doi.org/10.1113/jphysiol.1987.sp016671>
- Damascono RS, Takakura AC, Moreira TS (2014) Regulation of the chemosensory control of breathing by Kolliker-Fuse neurons. *Am J Physiol Regul Integr Comp Physiol* 307(1):R57–67. <https://doi.org/10.1152/ajpregu.00024.2014>
- Dawid Milner MS, Lara JP, Lopez de Miguel MP, Lopez-Gonzalez MV, Spyer KM, Gonzalez-Baron S (2003) A5 region modulation of the cardiorespiratory responses evoked from parabrachial cell bodies in the anaesthetised rat. *Brain Res* 982(1):108–118. [https://doi.org/10.1016/s0006-8993\(03\)03005-1](https://doi.org/10.1016/s0006-8993(03)03005-1)
- Dereli AS, Yaseen Z, Carrive P, Kumar NN (2019) Adaptation of respiratory-related brain regions to long-term hypercapnia: focus on neuropeptides in the RTN. *Front Neurosci* 13:1343. <https://doi.org/10.3389/fnins.2019.01343>
- Ellenberger HH, Feldman JL (1990) Brainstem connections of the rostral ventral respiratory group of the rat. *Brain Res* 513(1):35–42. [https://doi.org/10.1016/0006-8993\(90\)91086-v](https://doi.org/10.1016/0006-8993(90)91086-v)
- Ezure K (1990) Synaptic connections between medullary respiratory neurons and considerations on the genesis of respiratory rhythm. *Prog Neurobiol* 35(6):429–450. [https://doi.org/10.1016/0301-0082\(90\)90030-k](https://doi.org/10.1016/0301-0082(90)90030-k)
- Ezure K, Tanaka I (2006) Distribution and medullary projection of respiratory neurons in the dorsolateral pons of the rat. *Neuroscience* 141(2):1011–1023. <https://doi.org/10.1016/j.neuroscience.2006.04.020>
- Ezure K, Tanaka I, Kondo M (2003) Glycine is used as a transmitter by decrementing expiratory neurons of the ventrolateral medulla in the rat. *J Neurosci* 23(26):8941–8948. <https://doi.org/10.1523/JNEUROSCI.23-26-08941.2003>
- Fazekas EA, Morvai B, Zachar G, Dóra F, Székely T, Pogány Á, Dobolyi A (2020) Neuronal activation in zebra finch parents associated with reintroduction of nestlings. *J Comp Neurol* 528(3):363–379. <https://doi.org/10.1002/cne.24761>
- Feldman JL, Del Negro CA (2006) Looking for inspiration: new perspectives on respiratory rhythm. *Nat Rev Neurosci* 7(3):232–242. <https://doi.org/10.1038/nrn1871>
- Franklin KB, Paxinos G (2007) The mouse brain in stereotaxic coordinates, compact. Elsevier, Amsterdam
- Gang S, Sato Y, Kohama I, Aoki M (1995) Afferent projections to the Botzinger complex from the upper cervical cord and other respiratory related structures in the brainstem in cats: retrograde WGA-HRP tracing. *J Auton Nerv Syst* 56(1–2):1–7. [https://doi.org/10.1016/0165-1838\(95\)00049-x](https://doi.org/10.1016/0165-1838(95)00049-x)
- Geerling JC, Loewy AD (2006) Aldosterone-sensitive neurons in the nucleus of the solitary tract: efferent projections. *J Comp Neurol* 497(2):223–250. <https://doi.org/10.1002/cne.20993>
- Geerling JC, Kim M, Mahoney CE, Abbott SB, Agostinelli LJ, Garfield AS, Krashes MJ, Lowell BB, Scammell TE (2016) Genetic identity of thermosensory relay neurons in the lateral parabrachial nucleus. *Am J Physiol Regul Integr Comp Physiol* 310(1):R41–54. <https://doi.org/10.1152/ajpregu.00094.2015>
- Gray PA, Rekling JC, Bocchiaro CM, Feldman JL (1999) Modulation of respiratory frequency by peptidergic input to rhythmogenic neurons in the preBotzinger complex. *Science* 286(5444):1566–1568. <https://doi.org/10.1126/science.286.5444.1566>
- Gumbs MCR, Vuuregge AH, Eggels L, Unmehopa UA, Lamuadni K, Mul JD, la Fleur SE (2019) Afferent neuropeptide Y projections to the ventral tegmental area in normal-weight male Wistar rats. *J Comp Neurol* 527(16):2659–2674. <https://doi.org/10.1002/cne.24698>
- Guyenet PG, Mulkey DK, Stornetta RL, Bayliss DA (2005) Regulation of ventral surface chemoreceptors by the central respiratory pattern generator. *J Neurosci* 25(39):8938–8947. <https://doi.org/10.1523/jneurosci.2415-05.2005>
- Guyenet PG, Stornetta RL, Souza G, Abbott SBG, Shi Y, Bayliss DA (2019) The retrotrapezoid nucleus: central chemoreceptor and regulator of breathing automaticity. *Trends Neurosci* 42(11):807–824. <https://doi.org/10.1016/j.tins.2019.09.002>
- Haycock JW, Haycock DA (1991) Tyrosine hydroxylase in rat brain dopaminergic nerve terminals. Multiple-site phosphorylation in vivo and in synaptosomes. *J Biol Chem* 266(9):5650–5657. [https://doi.org/10.1016/S0021-9258\(19\)67644-1](https://doi.org/10.1016/S0021-9258(19)67644-1)
- Jiang C, Lipski J (1990) Extensive monosynaptic inhibition of ventral respiratory group neurons by augmenting neurons in the Botzinger complex in the cat. *Exp Brain Res* 81(3):639–648. <https://doi.org/10.1007/bf02423514>
- Joubert F, Loiseau C, Perrin-Terrin AS, Cayetanot F, Frugièr A, Vouron N, Bodineau L (2016) Key brainstem structures activated

- during hypoxic exposure in one-day-old mice highlight characteristics for modeling breathing network in premature infants. *Front Physiol* 7:609. <https://doi.org/10.3389/fphys.2016.00609>
- Kaneshige M, Shibata KI, Matsubayashi J, Mitani A, Furuta T (2018) A descending circuit derived from the superior colliculus modulates vibrissal movements. *Front Neural Circuits* 12:100. <https://doi.org/10.3389/fncir.2018.00100>
- Kansy JW, Daubner SC, Nishi A, Sotogaku N, Lloyd MD, Nguyen C, Lu L, Haycock JW, Hope BT, Fitzpatrick PF, Bibb JA (2004) Identification of tyrosine hydroxylase as a physiological substrate for Cdk5. *J Neurochem* 91(2):374–384. <https://doi.org/10.1111/j.1471-4159.2004.02723.x>
- Kaur S, Pedersen NP, Yokota S, Hur EE, Fuller PM, Lazarus M et al (2013) Glutamatergic signaling from the parabrachial nucleus plays a critical role in hypercapnic arousal. *J Neurosci* 33(18):7627–7640. <https://doi.org/10.1523/JNEUROSCI.0173-13.2013>
- Kc P, Haxhiu MA, Tolentino-Silva FP, Wu M, Trouth CO, Mack SO (2002) Paraventricular vasopressin-containing neurons project to brain stem and spinal cord respiratory-related sites. *Respir Physiol Neurobiol* 133(1–2):75–88. [https://doi.org/10.1016/s1569-9048\(02\)00131-3](https://doi.org/10.1016/s1569-9048(02)00131-3)
- Kline DD, King TL, Austgen JR, Heesch CM, Hasser EM (2010) Sensory afferent and hypoxia-mediated activation of nucleus tractus solitarius neurons that project to the rostral ventrolateral medulla. *Neuroscience* 167(2):510–527. <https://doi.org/10.1016/j.neuroscience.2010.02.012>
- Kohl J, Babayan BM, Rubinstein ND, Autry AE, Marin-Rodriguez B, Kapoor V et al (2018) Functional circuit architecture underlying parental behaviour. *Nature* 556(7701):326–331. <https://doi.org/10.1038/s41586-018-0027-0>
- Koshiya N, Smith JC (1999) Neuronal pacemaker for breathing visualized in vitro. *Nature* 400(6742):360–363. <https://doi.org/10.1038/22540>
- Kumar NN, Bowman BR, Goodchild AK (2012) Combined in situ hybridization and immunohistochemistry in rat brain tissue using digoxigenin-labeled riboprobes. *Neuromethods* 70:31–52. [https://doi.org/10.1007/978-1-61779-897-9\\_2](https://doi.org/10.1007/978-1-61779-897-9_2)
- Kuteeva E, Calza L, Holmberg K, Theodorsson E, Ogren SO, Hokfelt T (2004) Distribution of galanin and galanin transcript in the brain of a galanin-overexpressing transgenic mouse. *J Chem Neuroanat* 28(4):185–216. <https://doi.org/10.1016/j.jchemneu.2004.06.004>
- Lahiri S, Mulligan E, Andronikou S, Shirahata M, Mokashi A (1987) Carotid body chemosensory function in prolonged normobaric hyperoxia in the cat. *J Appl Physiol* (1985) 62(5):1924–1931. <https://doi.org/10.1152/jappl.1987.62.5.1924>
- Langer TM 3rd, Neumueller SE, Crumley E, Burgraff NJ, Talwar S, Hodges MR et al (2017a) Effects on breathing of agonists to mu-opioid or GABAA receptors dialyzed into the ventral respiratory column of awake and sleeping goats. *Respir Physiol Neurobiol* 239:10–25. <https://doi.org/10.1016/j.resp.2017.01.007>
- Langer TM 3rd, Neumueller SE, Crumley E, Burgraff NJ, Talwar S, Hodges MR et al (2017) State-dependent and independent effects of dialyzing excitatory neuromodulator receptor antagonists into the ventral respiratory column. *J Appl Physiol* (1985) 122(2):327–338. <https://doi.org/10.1152/japplphysiol.00619.2016>
- Lazarenko RM, Milner TA, Depuy SD, Stornetta RL, West GH, Kievits JA et al (2009) Acid sensitivity and ultrastructure of the retrotrapezoid nucleus in Phox2b-EGFP transgenic mice. *J Comp Neurol* 517(1):69–86. <https://doi.org/10.1002/cne.22136>
- Le S, Turner AJ, Parker LM, Burke PG, Kumar NN, Goodchild AK, McMullan S (2016) Somatostatin 2a receptors are not expressed on functionally identified respiratory neurons in the ventral respiratory column of the rat. *J Comp Neurol* 524(7):1384–1398. <https://doi.org/10.1002/cne.23912>
- Li N, Li A, Nattie E (2013) Focal microdialysis of CO<sub>2</sub> in the perifornical-hypothalamic area increases ventilation during wakefulness but not NREM sleep. *Respir Physiol Neurobiol* 185(2):349–355. <https://doi.org/10.1016/j.resp.2012.09.007>
- Li P, Janczewski WA, Yackle K, Kam K, Pagliardini S, Krasnow MA, Feldman JL (2016) The peptidergic control circuit for sighing. *Nature* 530(7590):293–297. <https://doi.org/10.1038/nature16964>
- Liu YY, Wong-Riley MT, Liu JP, Wei XY, Jia Y, Liu HL et al (2004) Substance P and enkephalineric synapses onto neurokinin-1 receptor-immunoreactive neurons in the pre-Botzinger complex of rats. *Eur J Neurosci* 19(1):65–75. <https://doi.org/10.1111/j.1460-9568.2004.03099.x>
- Mack SO, Wu M, Kc P, Haxhiu MA (2007) Stimulation of the hypothalamic paraventricular nucleus modulates cardiorespiratory responses via oxytocinergic innervation of neurons in pre-Botzinger complex. *J Appl Physiol* (1985) 102(1):189–199. <https://doi.org/10.1152/japplphysiol.00522.2006>
- Marcante AB, Wang LA, Little JT, Cunningham JT (2020) Caspase lesions of PVN-projecting MnPO neurons block the sustained component of CIH-induced hypertension in adult male rats. *Am J Physiol Heart Circ Physiol* 318(1):H34–H48. <https://doi.org/10.1152/ajpheart.00350.2019>
- Morinaga R, Nakamuta N, Yamamoto Y (2019) Serotonergic projections to the ventral respiratory column from raphe nuclei in rats. *Neurosci Res* 143:20–30. <https://doi.org/10.1016/j.neures.2018.05.004>
- Muere C, Neumueller S, Olesiak S, Miller J, Hodges MR, Pan L, Forster HV (2015a) Blockade of neurokinin-1 receptors in the ventral respiratory column does not affect breathing but alters neurochemical release. *J Appl Physiol* (1985) 118(6):732–741. <https://doi.org/10.1152/japplphysiol.00884.2014>
- Muere C, Neumueller S, Olesiak S, Miller J, Langer T, Hodges MR et al (2015b) Combined unilateral blockade of cholinergic, peptidergic, and serotonergic receptors in the ventral respiratory column does not affect breathing in awake or sleeping goats. *J Appl Physiol* (1985) 119(3):308–320. <https://doi.org/10.1152/japplphysiol.00145.2015>
- Mulkey DK, Stornetta RL, Weston MC, Simmons JR, Parker A, Bayliss DA, Guyenet PG (2004) Respiratory control by ventral surface chemoreceptor neurons in rats. *Nat Neurosci* 7(12):1360–1369. <https://doi.org/10.1038/mn1357>
- Mulkey DK, Talley EM, Stornetta RL, Siegel AR, West GH, Chen X, Sen N, Mistry AM, Guyenet PG, Bayliss DA (2007) TASK channels determine pH sensitivity in select respiratory neurons but do not contribute to central respiratory chemosensitivity. *J Neurosci* 27(51):14049–14058. <https://doi.org/10.1523/JNEUROSCI.4254-07.2007>
- Nagashimada M, Ohta H, Li C, Nakao K, Uesaka T, Brunet JF et al (2012) Autonomic neurocristopathy-associated mutations in Phox2b dysregulate Sox10 expression. *J Clin Invest* 122(9):3145–3158. <https://doi.org/10.1172/JCI63401>
- Nattie EE, Li A (2002) CO<sub>2</sub> dialysis in nucleus tractus solitarius region of rat increases ventilation in sleep and wakefulness. *J Appl Physiol* (1985) 92(5):2119–2130. <https://doi.org/10.1152/japplphysiol.01128.2001>
- Nattie E, Li A (2010) Central chemoreception in wakefulness and sleep: evidence for a distributed network and a role for orexin. *J Appl Physiol* (1985) 108(5):1417–1424. <https://doi.org/10.1152/japplphysiol.01261.2009>
- Nattie E, Li A (2012) Central chemoreceptors: locations and functions. *Compr Physiol* 2(1):221–254. <https://doi.org/10.1002/cphy.c100083>
- Nitsos I, Walker DW (1999) The distribution of Fos-immunoreactive neurons in the brainstem, midbrain and diencephalon of fetal sheep in response to acute hypoxia in mid and late gestation.



- Brain Res Dev Brain Res 114(1):9–26. [https://doi.org/10.1016/s0165-3806\(99\)00010-3](https://doi.org/10.1016/s0165-3806(99)00010-3)
- Nobis WP, Schuele S, Templar JW, Zhou G, Lane G, Rosenow JM, Zelano C (2018) Amygdala-stimulation-induced apnea is attention and nasal-breathing dependent. *Ann Neurol* 83(3):460–471. <https://doi.org/10.1002/ana.25178>
- Nunez-Abades PA, Morillo AM, Pasaro R (1993) Brainstem connections of the rat ventral respiratory subgroups: afferent projections. *J Auton Nerv Syst* 42(2):99–118. [https://doi.org/10.1016/0165-1838\(93\)90042-s](https://doi.org/10.1016/0165-1838(93)90042-s)
- Otake K, Ezure K, Lipski J, Wong She RB (1992) Projections from the commissural subnucleus of the nucleus of the solitary tract: an anterograde tracing study in the cat. *J Comp Neurol* 324(3):365–378. <https://doi.org/10.1002/cne.903240307>
- Ozaki I, Kurata K (2015) The effects of voluntary control of respiration on the excitability of the primary motor hand area, evaluated by end-tidal CO<sub>2</sub> monitoring. *Clin Neurophysiol* 126(11):2162–2169. <https://doi.org/10.1016/j.clinph.2014.12.032>
- Pouget P, Allard E, Poitou T, Raux M, Wattiez N, Similowski T (2018) Slower is higher: threshold modulation of cortical activity in voluntary control of breathing initiation. *Front Neurosci* 12:663. <https://doi.org/10.3389/fnins.2018.00663>
- Ptak K, Yamanishi T, Aungst J, Milescu LS, Zhang R, Richerson GB, Smith JC (2009) Raphe neurons stimulate respiratory circuit activity by multiple mechanisms via endogenously released serotonin and substance P. *J Neurosci* 29(12):3720–3737. <https://doi.org/10.1523/JNEUROSCI.5271-08.2009>
- Rekling JC, Feldman JL (1998) PreBotzinger complex and pacemaker neurons: hypothesized site and kernel for respiratory rhythm generation. *Annu Rev Physiol* 60:385–405. <https://doi.org/10.1146/annurev.physiol.60.1.385>
- Ribas-Salgueiro JL, Gaytan SP, Ribas J, Pasaro R (2005) Characterization of efferent projections of chemosensitive neurons in the caudal parapyramidal area of the rat brain. *Brain Res Bull* 66(3):235–248. <https://doi.org/10.1016/j.brainresbull.2005.05.014>
- Richter DW, Pierrefiche O, Lalley PM, Polder HR (1996) Voltage-clamp analysis of neurons within deep layers of the brain. *J Neurosci Methods* 67(2):121–123
- Rinaman L (2010) Ascending projections from the caudal visceral nucleus of the solitary tract to brain regions involved in food intake and energy expenditure. *Brain Res* 1350:18–34. <https://doi.org/10.1016/j.brainres.2010.03.059>
- Rosin DL, Chang DA, Guyenet PG (2006) Afferent and efferent connections of the rat retrotrapezoid nucleus. *J Comp Neurol* 499(1):64–89. <https://doi.org/10.1002/cne.21105>
- Saleeba C, Dempsey B, Le S, Goodchild A, McMullan S (2019) A student's guide to neural circuit tracing. *Front Neurosci* 13:897. <https://doi.org/10.3389/fnins.2019.00897>
- Sawczuk A, Mosier KM (2001) Neural control of tongue movement with respect to respiration and swallowing. *Crit Rev Oral Biol Med* 12(1):18–37. <https://doi.org/10.1177/10454411010120010101>
- Schaefer KE (1963) Respiratory adaptation to chronic hypercapnia. *Ann N Y Acad Sci* 109:772–782. <https://doi.org/10.1111/j.1749-6632.1963.tb13505.x>
- Schaefer KE, Hastings BJ, Carey CR, Nichols G Jr (1963) Respiratory acclimatization to carbon dioxide. *J Appl Physiol* 18:1071–1078. <https://doi.org/10.1152/jappl.1963.18.6.1071>
- Senthilkumaran M, Bobrovskaya L, Verberne AJM, Llewellyn-Smith IJ (2018) Insulin-responsive autonomic neurons in rat medulla oblongata. *J Comp Neurol* 526(16):2665–2682. <https://doi.org/10.1002/cne.24523>
- Shi Y, Stornetta DS, Reklow RJ, Sahu A, Wabara Y, Nguyen A, Li K, Zhang Y, Perez-Reyes E, Ross RA, Lowell BB, Stornetta RL, Funk GD, Guyenet PG, Bayliss DA (2021) A brainstem peptide system activated at birth protects postnatal breathing. *Nature* 589(7842):426–430. <https://doi.org/10.1038/s41586-020-2991-4>
- Smith JC, Ellenberger HH, Ballanyi K, Richter DW, Feldman JL (1991) Pre-Botzinger complex: a brainstem region that may generate respiratory rhythm in mammals. *Science* 254(5032):726–729. <https://doi.org/10.1126/science.1683005>
- Smith JC, Butera RJ, Koshiya N, Del Negro C, Wilson CG, Johnson SM (2000) Respiratory rhythm generation in neonatal and adult mammals: the hybrid pacemaker-network model. *Respir Physiol* 122(2–3):131–147. [https://doi.org/10.1016/s0034-5687\(00\)00155-9](https://doi.org/10.1016/s0034-5687(00)00155-9)
- Smith JC, Abdala AP, Rybak IA, Paton JF (2009) Structural and functional architecture of respiratory networks in the mammalian brainstem. *Philos Trans R Soc Lond B Biol Sci* 364(1529):2577–2587. <https://doi.org/10.1098/rstb.2009.0081>
- Spirovski D, Li Q, Pilowsky PM (2012) Brainstem galanin-synthesizing neurons are differentially activated by chemoreceptor stimuli and represent a subpopulation of respiratory neurons. *J Comp Neurol* 520(1):154–173. <https://doi.org/10.1002/cne.22723>
- Takakura AC, Moreira TS, Colombari E, West GH, Stornetta RL, Guyenet PG (2006) Peripheral chemoreceptor inputs to retrotrapezoid nucleus (RTN) CO<sub>2</sub>-sensitive neurons in rats. *J Physiol* 572(Pt 2):503–523. <https://doi.org/10.1113/jphysiol.2005.103788>
- Tenorio-Lopes L, Henry MS, Marques D, Tremblay ME, Drolet G, Bretzner F, Kinkead R (2017) Neonatal maternal separation opposes the facilitatory effect of castration on the respiratory response to hypercapnia of the adult male rat: evidence for the involvement of the medial amygdala. *J Neuroendocrinol*. <https://doi.org/10.1111/jne.12550>
- Teppema LJ, Veening JG, Kranenburg A, Dahan A, Berkenbosch A, Olivier C (1997) Expression of c-Fos in the rat brainstem after exposure to hypoxia and to normoxic and hyperoxic hypercapnia. *J Comp Neurol* 388(2):169–190. [https://doi.org/10.1002/\(SICI\)1096-9861\(19971117\)388:2](https://doi.org/10.1002/(SICI)1096-9861(19971117)388:2)
- Terreberry RR, Oguri M, Harper RM (1995) State-dependent respiratory and cardiac relationships with neuronal discharge in the bed nucleus of the stria terminalis. *Sleep* 18(3):139–144. <https://doi.org/10.1093/sleep/18.3.139>
- Tian GF, Peever JH, Duffin J (1999) Botzinger-complex, bulbospinal expiratory neurones monosynaptically inhibit ventral-group respiratory neurones in the decerebrate rat. *Exp Brain Res* 124(2):173–180. <https://doi.org/10.1007/s002210050612>
- Verner TA, Pilowsky PM, Goodchild AK (2008) Retrograde projections to a discrete apneic site in the midline medulla oblongata of the rat. *Brain Res* 1208:128–136. <https://doi.org/10.1016/j.brainres.2008.02.028>
- Weston MC, Stornetta RL, Guyenet PG (2004) Glutamatergic neuronal projections from the marginal layer of the rostral ventral medulla to the respiratory centers in rats. *J Comp Neurol* 473(1):73–85. <https://doi.org/10.1002/cne.20076>
- Wu Z, Autry AE, Bergan JF, Watabe-Uchida M, Dulac CG (2014) Galanin neurons in the medial preoptic area govern parental behaviour. *Nature* 509(7500):325–330. <https://doi.org/10.1038/nature13307>
- Yokota S, Kaur S, VanderHorst VG, Saper CB, Chamberlin NL (2015) Respiratory-related outputs of glutamatergic, hypercapnia-responsive parabrachial neurons in mice. *J Comp Neurol* 523(6):907–920. <https://doi.org/10.1002/cne.23720>
- Young JK, Wu M, Manaye KF, Kc P, Allard JS, Mack SO, Haxhiu MA (2005) Orexin stimulates breathing via medullary and spinal pathways. *J Appl Physiol* (1985) 98(4):1387–1395. <https://doi.org/10.1152/japplphysiol.00914.2004>